JGR Atmospheres

INTRODUCTION

10.1029/2023JD040581

Special Collection:
Probing the open ocean with the research sailing yacht Eugen Seibold for climate geochemistry

Key Points:

- New research platform for contamination-free sampling of the water column and atmosphere of biological, chemical, and physical properties
- Comprehensive marine geochemical analyzes including carbon (e.g., CO_2) in air and sea surface
- Proxy calibration of paleoclimate archives at high temporal and spatial resolution in relation to seawater and atmospheric parameters

Correspondence to:
R. Schiebel,
ralf.schiebel@mpic.de

Citation:
Schiebel, R., Aardema, H. M., Calleja, M. Ll., Dragoneas, A., Heins, L., Hrabe de Angelis, I., et al. (2024). Preface: Special issue on probing the open ocean with the research sailing Yacht *Eugen Seibold* for climate geochemistry. *Journal of Geophysical Research: Atmospheres*, *129*, e2023JD040581. https://doi.org/10.1029/2023JD040581

Received 11 JUL 2024
Accepted 11 JUL 2024

Author Contributions:
Conceptualization: Ralf Schiebel, Hedy M. Aardema, Maria Ll. Calleja, Antonis Dragoneas, Lena Heins, Isabella Hrabe de Angelis, Christopher Pöhlker, Hans Slagter, Hubert Vonhof, Yafang Cheng, Thomas Disper, Bernhard M. Fuchs, Steve Galer, Alfredo Martínez-García, Bettina Weber, Rudolf Amann, Ulrich Pöschl, Gerald H. Haug
Data curation: Hans Slagter, David Walter
Formal analysis: Ralf Schiebel, Hedy M. Aardema, Maria Ll. Calleja, Lena Heins, Isabella Hrabe de Angelis, Hans Slagter, Hubert Vonhof, Anthea I. Arns, Nils Adolphs, Alexandra Auderset, Sanja Basic, Aaron Bieler, Sonia Chaabane, Alexa Fischer, Bernhard

Preface: Special Issue on Probing the Open Ocean With the Research Sailing Yacht *Eugen Seibold* for Climate Geochemistry

Ralf Schiebel[1], Hedy M. Aardema[1,2], Maria Ll. Calleja[1,3], Antonis Dragoneas[1], Lena Heins[1], Isabella Hrabe de Angelis[1], Christopher Pöhlker[1], Hans Slagter[1], Hubert Vonhof[1], David Walter[1], Anthea I. Arns[1], Nils Adolphs[4], Alexandra Auderset[1], Sanja Basic[1], Aaron Bieler[1], Jan D. Brüwer[5], Sonia Chaabane[1,6,7], Yafang Cheng[1], Michal T. Chiliński[8], Jonathan D. Cybulski[1,9,10], Thomas Disper[1], Nicolas Duprey[1], Gregor Eichele[11], Björn Fiedler[12], Alexa Fischer[1], Alan D. Foreman[1], Bernhard M. Fuchs[5], Steve Galer[1], Jana Härri[1,13], Klaus Peter Jochum[1], Adrian Jost[1], Jonathan Jung[1], Henry Kleta[14], Gerhard Lammel[1,15], Otto Larink[16], Patrick Leibold[17], Alfredo Martínez-García[1], Simone Moretti[1], Jann-Gerrit Müller[4], Björn Nillius[1], Xihao Pan[1], Subha S. Raj[1], Janne Repschläger[1], Elizandro Rodrigues[18], S. Emil Ruff[19], Mareike Schmitt[1], Janine L. Schmitter[2], Andrew Sellers Lara[9], Péricles Silva[18], Sandi M. Smart[1,20], Matthias Sörgel[1], Brigitte Stoll[1], Hang Su[1], Meike Vogt[13], Tanja Wald[1], Bettina Weber[1,21], Jens Weber[1,21], Ulrike Weis[1], Rudolf Amann[5], Javier Arístegui[22], Thorsten Dittmar[3], Melchor González[22], Aaron O'Dea[9,23], Ulrich Pöschl[1], and Gerald H. Haug[1,2]

[1]Max Planck Institute for Chemistry, Mainz, Germany, [2]Department of Earth Sciences, ETH Zurich, Zurich, Switzerland, [3]Department of Biology, Universitat de les Illes Balears (UIB), Palma de Mallorca, Spain, [4]University of Oldenburg, Oldenburg, Germany, [5]Max Planck Institute for Marine Microbiology, Bremen, Germany, [6]FRB-Cesab, Institut Bouisson Bertrand, Montpellier, France, [7]CEREGE, Technopôle Environnement Arbois Méditerranée, Aix en Provence Cedex 04, France, [8]University of Warsaw, Warsaw, Poland, [9]Smithsonian Tropical Research Institute, Balboa, Republic of Panamá, [10]Graduate School of Oceanography, University of Rhode Island, Narragansett, RI, USA, [11]Max Planck Institute for Multidisciplinary Sciences, Göttingen, Germany, [12]Chemical Oceanography, GEOMAR, Helmholtz-Centre for Ocean Research Kiel, Kiel, Germany, [13]Department of Environmental Systems Science, ETH Zurich, Zurich, Switzerland, [14]Deutscher Wetterdienst, Hamburg, Germany, [15]Faculty of Science, RECETOX, Masaryk University, Brno, Czech Republic, [16]Zoologisches Institut, Technische Universität Braunschweig, Braunschweig, Germany, [17]Underwater Robotics Group, GEOMAR Helmholtz Centre for Ocean Research Kiel, Kiel, Germany, [18]Instituto do Mar (IMar), Mindelo, Republic of Cabo Verde, [19]Marine Biological Laboratory, Ecosystems Center/Josephine Bay Paul Center, Woods Hole, MA, USA, [20]Department of Geological Sciences, The University of Alabama, Tuscaloosa, AL, USA, [21]Institute for Biology, University of Graz, Graz, Austria, [22]Instituto de Oceanografía y Cambio Global, Universidad de Las Palmas de Gran Canaria, Las Palmas de Gran Canaria, Spain, [23]Sistema Nacional de Investigación, SENAYT, Balboa, Republic of Panamá

Abstract The 72-foot sailing yacht *Eugen Seibold* is a new research platform for contamination-free sampling of the water column and atmosphere for biological, chemical, and physical properties, and the exchange processes between the two realms. Ultimate goal of the project is a better understanding of the modern and past ocean and climate. Operations started in 2019 in the Northeast Atlantic, and will focus on the Tropical Eastern Pacific from 2023 until 2025. Laboratories for air and seawater analyses are equipped with down-sized and automated state-of-the-art technology for a comprehensive description of the marine carbon system including CO_2 concentration in the air and sea surface, pH, macro-, and micro-nutrient concentration (e.g., Fe, Cd), trace metals, and calcareous plankton. Air samples are obtained from ca. 13 m above sea surface and analyzed for particles (incl. black carbon and aerosols) and greenhouse gases. Plankton nets and seawater probes are deployed over the custom-made A-frame at the stern of the boat. Near Real-Time Transfer of underway data via satellite connection allows dynamic expedition planning to maximize gain of information. Data and samples are analyzed in collaboration with the international expert research community. Quality controlled data are published for open access. The entire suite of data facilitates refined proxy calibration of paleoceanographic and paleoclimate archives at high temporal and spatial resolution in relation to seawater and atmospheric parameters.

Plain Language Summary The new research sailing yacht *Eugen Seibold* (*ES*) enables clean, contamination-free sampling of air and seawater to better understand the interactions between ocean and

M. Fuchs, Steve Galer, Jana Härri, Klaus Peter Jochum, Gerhard Lammel, Simone Moretti, Jann-Gerrit Müller, Xihao Pan, Subha S. Raj, Janne Repschläger, S. Emil Ruff, Sandi M. Smart, Hang Su, Meike Vogt, Jens Weber
Funding acquisition: Ralf Schiebel, Gerald H. Haug
Investigation: Ralf Schiebel, Hedy M. Aardema, Maria Ll. Calleja, Lena Heins, Isabella Hrabe de Angelis, Christopher Pöhlker, Hans Slagter, Nils Adolphs, Sanja Basic, Jan D. Brüwer, Jonathan D. Cybulski, Nicolas Duprey, Gregor Eichele, Alan D. Foreman, Jana Härri, Jonathan Jung, Otto Larink, Janine L. Schmitter, Andrew Sellers Lara, Jens Weber
Methodology: Ralf Schiebel, Hedy M. Aardema, Maria Ll. Calleja, Antonis Dragoneas, Lena Heins, Isabella Hrabe de Angelis, Christopher Pöhlker, Hans Slagter, Hubert Vonhof, Aaron Bieler, Yafang Cheng, Michal T. Chiliński, Thomas Disper, Björn Fiedler, Bernhard M. Fuchs, Steve Galer, Jana Härri, Klaus Peter Jochum, Gerhard Lammel, Patrick Leibold, Alfredo Martínez-García, Björn Nillius, Janne Repschläger, Mareike Schmitt, Sandi M. Smart, Matthias Sörgel, Brigitte Stoll, Tanja Wald, Bettina Weber, Ulrike Weis, Ulrich Pöschl, Gerald H. Haug
Project administration: Ralf Schiebel, Antonis Dragoneas, Gerald H. Haug
Resources: Ralf Schiebel, Christopher Pöhlker, Hubert Vonhof, Yafang Cheng, Jonathan D. Cybulski, Steve Galer, Klaus Peter Jochum, Adrian Jost, Henry Kleta, Alfredo Martínez-García, Janne Repschläger, Elizandro Rodrigues, Andrew Sellers Lara, Péricles Silva, Bettina Weber, Rudolf Amann, Javier Arístegui, Thorsten Dittmar, Melchor González, Aaron O'Dea, Ulrich Pöschl, Gerald H. Haug
Supervision: Ralf Schiebel, Christopher Pöhlker, Hubert Vonhof, Yafang Cheng, Bernhard M. Fuchs, Klaus Peter Jochum, Alfredo Martínez-García, Bettina Weber, Rudolf Amann, Thorsten Dittmar, Aaron O'Dea, Ulrich Pöschl, Gerald H. Haug
Validation: Ralf Schiebel, Hedy M. Aardema, Maria Ll. Calleja, Lena Heins, Isabella Hrabe de Angelis, Christopher Pöhlker, Hans Slagter, Hubert Vonhof, David Walter, Aaron Bieler, Yafang Cheng, Klaus Peter Jochum, Alfredo Martínez-García, Bettina Weber
Visualization: Ralf Schiebel, Hedy M. Aardema, Maria Ll. Calleja, Lena Heins, Isabella Hrabe de Angelis, Christopher Pöhlker, Hans Slagter, Hubert Vonhof, Anthea I. Arns, Aaron Bieler, Björn Fiedler, Patrick Leibold, Xihao Pan, Subha S. Raj, Jens Weber

climate. For example, the oceans remove increasingly less carbon dioxide (CO_2) from the atmosphere the more saturated they are with CO_2 (ocean acidification). However, a detailed systematic understanding of air-sea exchange processes remains to be developed. We analyze air and seawater as well as the exchange of greenhouse gases and other substances such as aerosols and soot (black carbon) between air and seawater at high resolution using modern materials and technologies. Scaled-down, energy-efficient, and automated probes developed over the past decade are being used to measure around 50 different characteristics of the marine environment. The work deck at the stern of the boat allows the use of custom-made water samplers and plankton nets to study the ocean to below 1,000 m depth. In addition, the new data enables a better understanding of past ocean archives, such as the marine plankton accumulated in seafloor sediments, to reconstruct past climate changes. From 2019 to 2022, the *S/Y ES* sailed in the eastern North Atlantic and will operate in the tropical eastern Pacific until 2025.

1. Background and Summary

The open ocean has been sampled since the mid 19th century onwards with an international fleet of ships (e.g., Thomson & Murray, 1886). Since the early 20th century, diesel-powered vessels have been employed to sample the physical, chemical, and biological state and composition of the oceans for a better hydrological, ecological, climatological, and paleoceanographic understanding of the Earth system. Expeditions have been funded by national agencies, and advance planning of typically two to 3 years have been required to establish a logistic and financial basis. From the early 2000s, sailing yachts such as the *Sorcerer II* (Gross, 2007) have been employed for targeted sampling of plankton and other properties of the surface water column, and allow dynamic short-to-mid-term planning at much smaller budgets than needed for the larger vessels coordinated by the governmental panels. As a results, projects such as *Tara Oceans* (e.g., Pesant et al., 2015) have provided previously inaccessible insights into the ecology and carbon turnover of the surface ocean, with a global focus on metagenomics and plankton biodiversity (Biard et al., 2016; de Vargas et al., 2015; Guidi et al., 2016).

The *S/Y Eugen Seibold* (*ES*, Figure 1), call sign CRA7241, is the latest addition to the international fleet of small research vessels designed for targeted sampling of the blue ocean for a better understanding of the ocean environment including the overlying atmosphere, air-sea exchange processes at the regional to global scale, and multi-parameter calibration of marine planktic archives and paleo-proxies. It is meant to foster the scientific understanding of the modern oceans, and to improve reconstruction of oceanographic and climatic conditions over past climate cycles. The *S/Y ES* project is part of the EU funded *AtlantECO* (atlanteco.eu) and the German *DAM-Underway-Research Data* (allianz-meeresforschung.de), which provide frameworks of resources to support a global understanding of the changing oceans.

The sailing vessel provides clean conditions for continuous collective contamination-free (C^3s) sampling of both atmosphere and ocean, with a maximum autonomy of combustion-free "clean" sailing of 14 hr provided by a 65 kWh battery (Table 1). The scientific infrastructure includes trace metal clean polytetrafluorethylene (PTFE) inlets for sampling the atmosphere and ocean, laboratories, and probes for in situ sampling of the surface water column (Table 2). The full navigational and scientific setup was tested, and the first deep water site was sampled on 10 April 2019. Following adjustments for the compatibility of the many different probes for air and water analyses (Table 2), such as alternating CO_2 measurements from air and surface ocean, a North-to-South transect was sampled in the eastern North Atlantic in 2020 and 2021 (Table 3).

The *S/Y ES* expeditions along the *20-West-Transect* comprise 15 targeted scientific campaigns in 2020 and 2021 (Table 3), plus six educational cruises with students from European (mostly Swiss and German) and West African (WASCAL-CV, Mindelo, São Vicente, Cabo Verde) universities. The transect spans the eastern North Atlantic (Figure 2) and provides an integrated high-resolution multi- and cross-disciplinary approach to the climate biogeochemistry of the modern ocean and overlying atmosphere, for a better understanding of air-sea exchange processes that affect climate at the regional to global scale.

In the following, we provide a technological and conceptual overview of the research platform and the scientific perspectives of the project. First data from the campaigns to the Northeast Atlantic are presented and discussed for the scientific significance, and the further perspective of this project and similar projects in development for better understanding of

Writing – original draft: Ralf Schiebel, Hedy M. Aardema, Maria Ll. Calleja, Antonis Dragoneas, Lena Heins, Isabella Hrabe de Angelis, Christopher Pöhlker, Hans Slagter, Hubert Vonhof, David Walter, Sanja Basic, Aaron Bieler, Yafang Cheng, Björn Fiedler, Alexa Fischer, Patrick Leibold, Alfredo Martínez-García, Xihao Pan, Subha S. Raj, Sandi M. Smart, Bettina Weber, Jens Weber, Ulrich Pöschl
Writing – review & editing: Ralf Schiebel, Hedy M. Aardema, Maria Ll. Calleja, Lena Heins, Christopher Pöhlker, Hans Slagter, David Walter, Anthea I. Arns, Aaron Bieler, Yafang Cheng

- the physical, chemical, and biological properties of the surface ocean and lower atmosphere at a high temporal (second) scale and spatial (meter scale), and
- the exchange processes between the two realms, which affect the regional and global climate, including
- a comprehensive description of the marine carbon system including CO_2 concentration in the air and sea surface.
- Subsequently, we aim for an improved calibration of paleoclimate proxies and archives in relation to seawater and atmospheric parameters.
- Ultimately, the new findings may be fed into numerical models to better predict future changes of the complex ocean and climate systems.

This article acts as an introduction to the JGR-Atmospheres and Earth and Space Science special section titled *Probing the open ocean with the research sailing yacht ES for climate geochemistry*. The respective analytical methodologies, sampling techniques, and data processing and management will be detailed in the topical papers emerging from the S/Y *ES* project.

Sampling is conveyed according to the Code of Conduct for Responsible Marine Research in the Deep Seas and High Seas of the OSPAR Maritime Area, and according to the Nagoya Protocol, that is, the UN convention on Access to Genetic Resources and the Fair and Equitable Sharing of Benefits Arising from their Utilization to the Convention on Biological Diversity.

In the following, data and samples obtained in the eastern North Atlantic are presented as an example of a systematic synoptic understanding of physical, chemical, and biological variables of the ocean climate as a major driver of global climate change (e.g., Steffen et al., 2020), facilitated by the technological infrastructure of the *S/Y ES*.

2. Technological Infrastructure

The scientific and navigational technology of the *S/Y ES* has been designed to be as facile as possible for easy and safe operation and maintenance at sea, and at minimum volume, size, and weight (Table 1), allowing for an autonomy of up to 20 days. Energy production and propulsion are aimed at the ecologically and economically most efficient use of resources and minimum emissions facilitating contamination-free sampling of the atmosphere and ocean. At favorable conditions, *S/Y ES* can achieve a ratio of 3:1 emission-free to combustion-emission time. Any air or water emission activity, such as the operation of the combustion engines, cooking, or bilge water pumping is automatically detected and logged by software running on the main control computer of the vessel, facilitating *a-posteriori* analysis of the scientific data and identification of potential data artifacts. A pack of 65 kWh $LiFePO_4$ batteries allows up to 14 hr of contamination free sampling, facilitated by a battery monitoring system and automation of the various operations (Table 1). A total generated electrical power of 25 kW allows for battery recharging in 4 hr.

2.1. Scientific Infrastructure

The layout of the *S/Y ES* is optimized for maximum laboratory and work space comprising about 50% of the boat's interior (Figure 3). The wet laboratory for seawater analyses at the starboard aft position of the boat is separated from the adjacent semi-dry laboratory, and a dry laboratory toward midship, respectively. The air-chemistry laboratory located at the rearward portside is hermetically separated from the other laboratories and the living quarters. Sea-going sampling and probing equipment is provided through a hatch (113.0 cm × 110.5 cm) from the garage at the aft of the boat, and separated from the boat's interior by a bulkhead (Figure 3).

2.2. Probing the Ocean

A pivoted hydraulic A-frame at the stern of the boat facilitates sampling of the water column, using a 6-mm *Dyneema* wire with a (theoretical) maximum length of 3,000 m. The wire is operated with a scientific winch (*CORMAC Q2 HS*, MacArtney A/S, Esbjerg, Denmark). A custom-made heave compensation-system allows smooth operation of the winch and wire, and deployment of sampling devices at considerable swell and wave movement. The A-frame is designed for picking up sampling gear of up to 100 kg (net weight under air) from the hatch of the garage under the work deck (5 m × 2.5 m), and pivoting it outboard to be operated in the water column. Typically, the rosette water sampler, in situ large volume pump, bongo net, and multinet (Table 2,

Table 1
Technical Data and Dimensions of the S/Y Eugen Seibold

Dimensions and occupation			
Length over all	L_{MAX}	23.87	m
Length of hull	L_H	21.86	m
Length of water line	L_{WL}	20.84	m
Width over all	B_{MAX}	6.00	m
Draft of hull	t_c	1.00	m
Draft, maximum	t_{MAX}	3.22	m
Height over water line	H_{MAX}	30.00	m
Maximum payload[a]	mmtl	6,734	kg
Displacement, empty	mlc	40,020	kg
Displacement, max	mldc	46,476	kg
Accommodation	Number	8	berth
Maximum occupation	Number	12	persons
Power supply and autonomy			
Main engine mechanical power output	$P_{flywheel}$	155	kW
Main engine electrical power output	$P_{alternators}$	15	kVA
Diesel genset electrical power output	P_{genset}	12	kVA
Wind generator electrical power output	P_{wind}	0.7	kW
Main battery capacity	$E_{battery}$	65	kWh
Maximum emission-free operation (no air-conditioning)	$t_{zero\text{-}emission}$	14	hr
Maximum emission-free operation (with air-conditioning in mid-latitudes)	$t_{zero\text{-}emission\text{-}A/C}$	7	hr
Total power delivery at 230 Vac	P_{230V}	16	kVA
230 Vac power available for scientific instruments	$P_{230V\text{-}science}$	4	kVA
Total power delivery at 24 Vdc	P_{24V}	11	kW
24 Vdc power available for scientific instruments	$P_{24V\text{-}science}$	2	kW
Sails			
Main sail	Sail area	125	m^2
Jib	Sail area	102	m^2
Storm jib	Sail area	20	m^2
Try sail	Sail area	30	m^2
Reacher	Sail area	215	m^2

[a]Maximum payload includes persons, materials, and liquids such as water and fuel. Supply voltages are 12 Vdc and 330 Vdc.

Figure 4) are lowered at 20 m per minute, and heaved at 30 m per minute, to allow for a straight line at each point of time. Flow meters and PT (pressure, temperature) probes are used to quantify water volumes sampled with the plankton nets, and provide information on sampling depths, respectively. Seawater and freshwater are provided at the work deck for rinsing and cleaning of the nets and other sampling gear.

Mesoplankton including foraminifers are collected with a suite of plankton nets (Table 2), hauled horizontally drifting at a speed of 1 knot (i.e., ca. 0.5 ms^{-1}), or hauled vertically at a speed of 20–30 m per minute (i.e., ca. 0.3–0.5 ms^{-1}) from the A-frame. Plankton nets with large apertures provide sufficient numbers of individuals (e.g., hundreds of foraminifers and pteropods) for assessment of the population dynamics and most chemical analyses. Towing strategies are adapted for varying types of samples to provide valuable ancillary data. The underway measurement and sampling program, for example, of water column depth profiles that are conducted at the same site and time as the tows, provide a wide suite of samples and data for proxy calibration including analyses of stable isotopes and element ratios of planktic foraminifers (Bieler, 2022; A. Fischer et al., 2024).

Table 2
Laboratories, Sensors, and Sampling Devices for Analyzing the Atmosphere and Ocean

	Brand	Purposes and parameters
Wet laboratory probes		
Flow Cytometer	CytoSense	Cell counts of bacterioplankton, phytoplankton, and zooplankton
FastOcean FRRF and Act2	Chelsea Technologies	Active chl-*a* fluorescence and derived parameters
Filtration Racks	MPIC	Various filtration racks for seawater analyses
Milli DI and Simplicity	Milli-Q	Deionized and ultraclean water for processing of samples
Freezers and Fridges	various brands	Freezing (−20°C) and cooling (+4°C to +8°C) of samples
FerryBox	SubCtech	Analyses of seawater from 3.2 m water depth (keel)
Thermosalinograph, SBE45	Sea-Bird Scientific	Water temperature and salinity in sampling chamber
In situ thermometer at the Hull	SoundNine Inc.	Water temperature at the hull
Oxygen Optode 4835	Aanderaa	Dissolved oxygen, oxygen air saturation, water temperature
ECO Triplet Fluorometer	WET Labs, Inc.	Chlorophyll, phycocyanin, CDOM
EnviroFlu Sensor	TriOS GmbH	Polycyclic Aromatic Hydrocarbons (PAH)
OPUS and UV Spectral Sensor	TriOS GmbH	NO_2, NO_3, DOCeq, SAC254, 10 mm path length
Turbidity Probe	Seapoint Sensors Inc.	Seawater turbidity
Glass Membrane pH Probe	Xylem Analytics	Seawater pH
MK2 pCO_2 analyzer with LI840x	LI-COR	CO_2 partial pressure in seawater and air
LISST 200X	Sequoia Scientific	Particle size distribution in seawater
Semi-dry laboratory		
Delta Ray™ Spectrometer	Thermo Scientific	$\delta^{13}C$ and $\delta^{18}O$ of CO_2, CO_2 concentration in surface seawater
MiniRUEDI Mass Spectrometer	Gasometrix	Oxygen (O_2), nitrogen (N_2), and argon (Ar) dissolved in seawater
Clean Bubble	MPIC	Clean bench for contamination-free handing of water samples
Deep Freezer	Sterling Ultracold	Deep freezing (−80°C) of samples, 25 L capacity
Air laboratory		
Low volume filter sampler, DPA14	Digitel AG	Air samples on 47 mm filters
Flow Sensor	Sensirion AG	Digital mass flow meter, measures air flow of Low Volume Sampler
Aethalometer, AE, Model AE33	Aerosol d.o.o.	Aerosol absorption coeff. at wavelengths between 370 and 950 nm
Aerodynamic Particle Sizer, APS	TSI Inc.	Aerosol particle number size distributions from 0.5 to 20 µm
Condensation Particle Counter, CPC[a]	TSI Inc.	Total number concentration of aerosol particles >5 nm in diameter
Data Logger	MSR	Monitoring T, humidity, air pressure and acceleration in the aerosol inlet line to the AE33, SP2, CPC, SMPS, and SIBS
Spectral Intensity Bioaerosol Sensor, SIBS[b]	DMT	Spectrally resolved fluorescence of single particles in real time
Scanning Mobility Particle Sizer™, SMPS[c,d]	TSI Inc.	Aerosol particle number size distributions from 0.01 to 0.45 µm
Single Particle Soot Photometer, SP2[e]	Droplet Measurement Technologies (DMT)	Mass conc., core diam., and coating thickness of refractory black carbon (rBC) particles
Captair Flowcap 700 Laminar Flow Cabinet	Cole-Parmer Ltd.	Clean bench for contamination-free handing of samples

Table 2
Continued

	Brand	Purposes and parameters
Deployables		
Rosette Water Sampler SlimLine	Hydro-Bios	5 × 5 L Niskin bottles for seawater samples
CTD48M	Sea and Sun Technology	Four sensors, incl. temperature (*T*), salinity (*S*), 6,000 m max. water depth
CTD75M	Sea and Sun Technology	Eight sensors, T, S, diss. O_2, chl-*a* fluores., pH, turbidity, PAR, 500 m max.
SV48M	Sea and Sun Technology	Temperature in the water column, attached to deployables
RBR Duet DT Logger	Nautilus	Temperature in the water column, attached to deployables
GoFlo Bottles	General Oceanics	3 × 5 L trace metal clean seawater samples
Large Volume Pump WTS-6-1-142LV	McLane	In situ seawater filtration over 142-mm filters for various analyses
Multi Net midi Ti	Hydro-Bios, MPIC	Mesoplankton including foraminifers, pteropods, copepods, >100 µm
Bongo Net	Hydro-Bios	Mesoplankton including foraminifers, pteropods, copepods, >100 µm
Apstein Net	Hydro-Bios	Phytoplankton, >20 µm
Sediment Trap	Hydro-Bios, MPIC	Sinking particles in the water column
Top of wheel house		
Bioaerosol Sampler, Coriolis® Micro	Bertin Technol. SAS	Biological air sampler with cyclone technology, high air flow (300 lpm)
Mast		
Top Box	LI-COR, SubCtech, MPIC	Photosynthetic Active Radiation (PAR)
Anemometer	Raymarine	Wind speed

Note. For the positions of laboratories and devices see Figure 3. MPIC indicates own developments at the Max Planck Institute for Chemistry. [a]Petäjä et al. (2006). [b]Könemann et al. (2019). [c]Knutson and Whitby (1975). [d]Franco et al. (2022). [e]Schwarz et al. (2006).

Despite of being important constituents of marine ecosystems much remains to be discovered about the in situ behavior of zooplankton, and in particular, about their circadian clocks which are implicated in behaviors such as daily vertical migration that influences macroscale ecological dynamics (Raghavan et al., 2023). The transcriptomes of 17 diverse marine zooplankton were sequenced, assembled de novo, and annotated. The transcriptomes were mined using a phylogenetics-based approach. Multiple sequences of interest are provided for multiple species identified simultaneously using de novo assembled transcriptomic data. OrthoFinder is being used with transcriptomic data to identify the orthologs of interest (Raghavan et al., 2023).

Water samples for characterization of the epipelagic and mesopelagic ocean are collected using the rosette water sampler equipped with five 5-L Niskin bottles and a CTD48M or CTD75M (Table 2). Vertical profiles of temperature, salinity, dissolved O_2, chlorophyll-*a* (chl-*a*) fluorescence, pH, and Photosynthetic Active Radiation (PAR; with the CTD75M, upper 200 m max.) are routinely produced at station, together with discrete seawater samples for macronutrients, chl-*a*, photophysiology, microbial cell abundance, molecular biology (DNA), nitrogen isotopes ($\delta^{15}N$), and biomarkers. In addition, *Teflon*-coated *Go-Flo* bottles (General Oceanics, Florida, US) are used for contamination free sampling of dissolved organic carbon (DOC) and trace metals (Table 2). In situ seawater filtration for trace metals and other materials is performed in the water column using the large volume pump (Table 2) equipped with three 142-mm filter-holders at a flow rate of 4 L min^{-1}. For contamination-free handling of wet and dry samples, a flexible clean bench (*clean bubble*) is available in the dry laboratory (Figure 3).

Continuous surface ocean sampling is facilitated by a *FerryBox* (*OceanPack*™, SubCtech, Kiel, Germany), which provides 5–7 L min^{-1} of seawater from the base of the keel (draft of 3.2 m water depth) through two half-inch diameter PTF tubes to the wet laboratory. Pristine samples for flow cytometry and phytoplankton photophysiology with a Fast Repetition Rate (FRR) fluorometer (*FastOcean FRRf*, Table 2), as well as discrete samples for various biogeochemical analyses are collected at the underpressure side of the system before a membrane pump (e.g., for nutrient analyses, DOC, chl-*a*, microbial cell abundance, DNA, $\delta^{15}N$, trace metals, and

Journal of Geophysical Research: Atmospheres 10.1029/2023JD040581

Table 3
Scientific Expeditions of S/Y Eugen Seibold (ES) in 2020 and 2021

Cruise number	Year (UTC)	Month (UTC)	Start day end day (UTC)	Start time end time (UTC)	Start port end port	CSS	Latitude longitude CSS	Water depth CSS (m)	Abbreviation CSS	UW samples (#)	Samples at station (#)	Air samples (#)
ES20C02	2020	6	23–26	02:00 18:00	Bremerhaven, Germany Torshavn, Faroe Islands	–	–	–	–	49	0	0
ES20C03	2020	7	2–3	06:00 21:00	Torshavn, Faroe Islands Seydisfjordur, Iceland	–	–	–	–	21	0	0
ES20C04	2020	7	10–15	11:00 08:00	Seydisfjordur, Iceland Vestmannaeyjar, Iceland	17	67.0000–6.0000	3,150	67N 6W GIN Seas	79	172	13
ES20C05	2020	7	20–24	07:00 20:00	Vestmannaeyjar, Iceland Galway, Ireland	18	57.0000–20.0000	1,070	57N 20W Rockall Trough	105	138	20
ES20C06	2020	8	7–14	07:00 13:00	Galway, Ireland Ponta Delgada, São Miguel, PT	19	47.0000–20.0000	4,630	47N 20W BIOTRANS	173	152	27
ES20C07	2020	8	21–24	14:00 18:00	Ponta Delgada, São Miguel, PT	20	37.0000–21.0000	4,860	37N 21W Azores Front	86	152	17
ES20C08	2020	9	17–22	12:00 09:00	Ponta Delgada, São Miguel, PT Quinta do Lorde, Madeira, PT	21	33.0000–22.0000	5,250	33N 22W Madeira Basin	121	159	19
ES20C09	2020	11	7–9	08:30 23:00	Funchal, Madeira, PT Marina Rubicon, Lanzarote, ES	22	29.5000–15.0000	3,560	ESTOC*	46	159	6
ES21C03	2021	2	21–23	18:30 19:00	Las Palmas, Gran Canarioa, ES Marina Rubicon, Lanzarote, ES	25	29.5000–15.0000	3,560	ESTOC*	15	140	19
ES21C06	2021	4	12–20	06:00 13:30	Marina Rubicon, Lanzarote, ES Mindelo, São Vicente, CV	28	21.0000–21.0000	4,140	21N 21W Mauretanian Upwelling	156	204	15
ES21C07	2021	5	1–2	14:00 20:00	Mindelo, São Vicente, CV	29	17.6000–24.3000	3,610	CVOO	0	145	3
ES21C08	2021	5	10–22	17:30 15:00	Mindelo, São Vicente, CV	30	3.0000 – 22.0000	4,410	3N 22W Equatorial Upwelling	342	204	40
ES21C11	2021	6	6–14	13:30 08:00	Mindelo, São Vicente, CV Las Palmas, Gran Canaria, ES	–	–	–	–	0	0	0
ES21C14	2021	9	8–10	15:00 03:00	Marina Rubicon, Lanzarote, ES	34	29.5000–15.0000	3,560	ESTOC*	0	84	3
ES21C16	2021	9	24–26	18:30 23:00	Marina Rubicon, Lanzarote, ES	36	29.5000–15.0000	3,560	ESTOC*	30	95	0

Note. Seven-digit campaign labels give ES Year Year (e.g., 20) Cruise (C) Digit1 Digit2 (D1D2) reading ESyyCD1D2. On expeditions without sampling of the deep water column at a central sampling site (CSS), underway samples from 3 m water depth (ocean) and 13 m altitude (air) were obtained. Negative latitudes and longitudes indicate southern and western hemispheres, respectively. Latitudes and longitudes give the targeted sampling sites, and actual samples were obtained adrift at some distance. PT is Portugal, ES is Spain, CV is Cape Verde Islands, GIN Seas is Greenland, Iceland, and Norwegian Seas (GINS), ESTOC* is near the European Station for Time-Series in the Ocean Canary Islands (ESTOC), CVOO is Cape Verde Ocean Observatory, UW is underway. For metadata on the expeditions see https://www.pangaea.de/expeditions/bybasis/Eugen%20Seibold (e.g., Walter et al., 2023). Master track available from https://doi.org/10.1594/PANGAEA.960382.

Figure 1. The *S/Y Eugen Seibold* under sails off Lanzarote Island. Air is sampled from ca. 13 m above sea surface at the top of the black tube behind the beam. Devices for sampling of the water column are deployed from the A-frame at the stern (see also Figure 3). Photo, D. Jack, MPIC.

biomarkers). The *FRRf* has been replaced by a *LabSTAF* (Chelsea Technologies Group Ltd, Molesey, UK) in 2022 for enhanced sensitivity and accuracy of the measurements.

A membrane pump delivers the seawater to the sampling chamber of the *FerryBox*, where the seawater is de-bubbled, and temperature, salinity, pH, fluorescence, dissolved oxygen (DO), and turbidity are measured (Table 2). A peristaltic pump distributes the sampled water to probes for the quantification of UV spectral shape (DOC_{eq}, NO_3, and NO_2; OPUS), pCO_2 (non-dispersive infrared LI-840 analyzer, LI-COR), and size spectrum of suspended particles (LISST 200X) in the seawater (Table 2). For continuous analyses of the pico-, nano-, and microplankton (<1 mm in diameter, and imaging of the larger cells), seawater is delivered from the *FerryBox* (before the membrane pump) to the *CytoSense* (CytoBuoy b.v., Woerden, The Netherlands) flow cytometer (Table 2). For quantification of oxygen (O_2), nitrogen (N_2), and argon (Ar) concentrations, seawater is delivered to a gas exchange module, and the equilibrated gas phase is sampled by the *miniRUEDI* mass spectrometer (Brennwald et al., 2016) in the adjacent semi-dry laboratory (Table 2).

Oxygen ($\delta^{18}O$) and carbon ($\delta^{13}C$) isotopes of the dissolved inorganic carbon (DIC) in seawater and calcareous plankton, including planktic foraminifer tests, are analyzed from discrete samples at the MPIC in Mainz (Vonhof et al., 2020). To provide high spatial and temporal resolution, DIC $\delta^{13}C$ data for the *S/Y ES* database, discrete seawater samples are stored in 4 mL glass bottles with a septum cap. Complementary $\delta^{18}O$ and $\delta^{2}H$ analyses are done on a separate 1.5 mL sample. Samples are taken in transit from the continuous surface sampling system (*FerryBox*), and with the Rosette water sampler from the water column when on station. The small total sample size allows for hundreds of samples to be collected and stored per cruise, providing the data density required for precise comparison with other shipboard data. Carbon isotope analysis is performed at the labs of the MPIC in Mainz using a Gasbench II preparation device coupled to a DeltaV mass spectrometer (Vonhof et al., 2020).

2.3. Probing the Atmosphere

Air for atmospheric observations is sampled behind the main sail, about 10 m above the work deck, which corresponds to a sampling height of about 13 m above water line. The inlet system consists of a flexible glass-epoxy tube with an outer diameter (O.D.) of 60 mm and an inner diameter (I.D.) of 56 mm (Prince Fiber Tech b.v., Dronten, The Netherlands), which guides an inner bundle of smaller inlet tubes of different materials and diameters. The inlet system has been designed and optimized to be resistant and stable under the harsh environmental conditions at sea, and shields the bundle of inlet tubes from heating through direct sunlight. The system

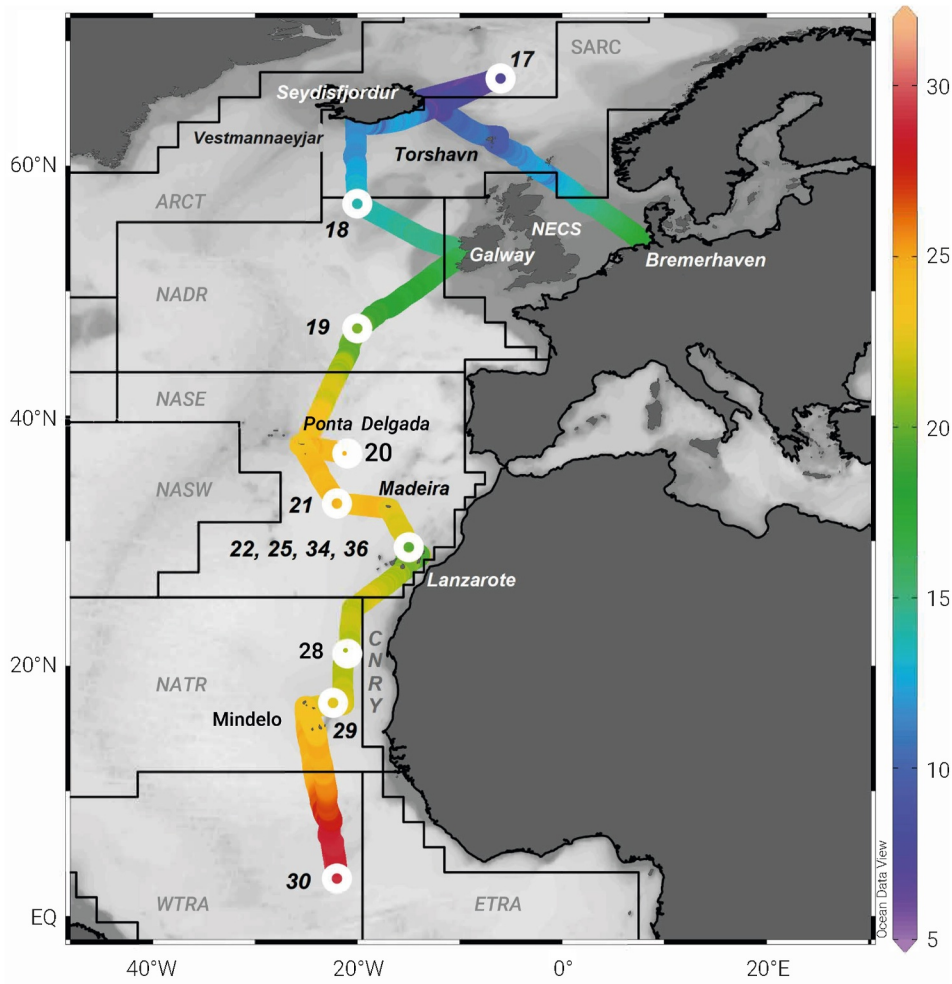

Figure 2. *S/Y Eugen Seibold* (*ES*) cruise track shown as sea surface temperature (°C). *S/Y ES* expeditions ES20C02 to ES21C16, from Bremerhaven in June 2020 to the equatorial upwelling in April/May 2021 (Table 3). More than 1,500 samples and several Terabytes of data at a one-second interval (meter scale) were obtained on more than 10,000 nautical miles (ca. 19,000 km). The sampling stations at 57°N, 47°N, 33°N, 29°N, 21°N, and 17°N have been sampled as part of a long-term monitoring program on the changing ocean and climate (Table 3, central sampling site). White circles show hydrocast stations. Metadata, environmental data, and sample lists have been recorded in the respective cruise reports available upon request. Metadata on the expeditions are available at https://www.pangaea.de/expeditions/bybasis/Eugen%20Seibold, including links to the master tracks, such as the master track of the Expedition ES19C01 (Walter et al., 2023). The boxes correspond to the biogeographic provinces detailed by Longhurst (2007). Image produced using Ocean Data View (Schlitzer, 2022).

allows for flexibility and modifications if changes in the instrument suite (Table 2) are implemented, to provide the smallest possible sampling losses in the aerosol observations according to von der Weiden et al. (2009). The inlet tube bundle consists of (a) four electrically conductive (i.e., carbon-primed) polyurethane tubes with 9.0 mm I.D. and 12.0 mm O.D. (Landefeld GmbH, Kassel, Germany) that together provide up to ∼50 L min^{-1} of air for filter sampling, (b) three electrically conductive polyurethane tubes with 3.9 mm I.D. and 6.0 mm O.D. that together provide up to ∼18 L min^{-1} of air for the online aerosol instrumentation, (c) a Synflex metalized tube with 4.0 mm I.D. and 6.0 mm O.D. (1300-M060E, G + S Schlauchtechnik GmbH, Hamburg, Germany) for greenhouse gas sampling, and (d) a flexible perfluoroalkoxy alkanes (PFA) tube with 4.0 mm I.D. and 6.4 mm O.D. (PFA-T4-047-100, Swagelok, Frankfurt a.M., Germany) for reactive trace gas sampling. All tubes are connected to a modified version of a total suspended *sigma 2* inlet head. The inner diameters of the aerosol inlet tubes and flow rates have been optimized to achieve low residence times of the sampled air, while maintaining laminar flow conditions (von der Weiden et al., 2009). The sampled air for the online aerosol instrumentation is dried to <30% relative humidity (RH) with a 60 cm long monotube Nafion dryer (type MD-700-24S-3, Perma Pure, USA).

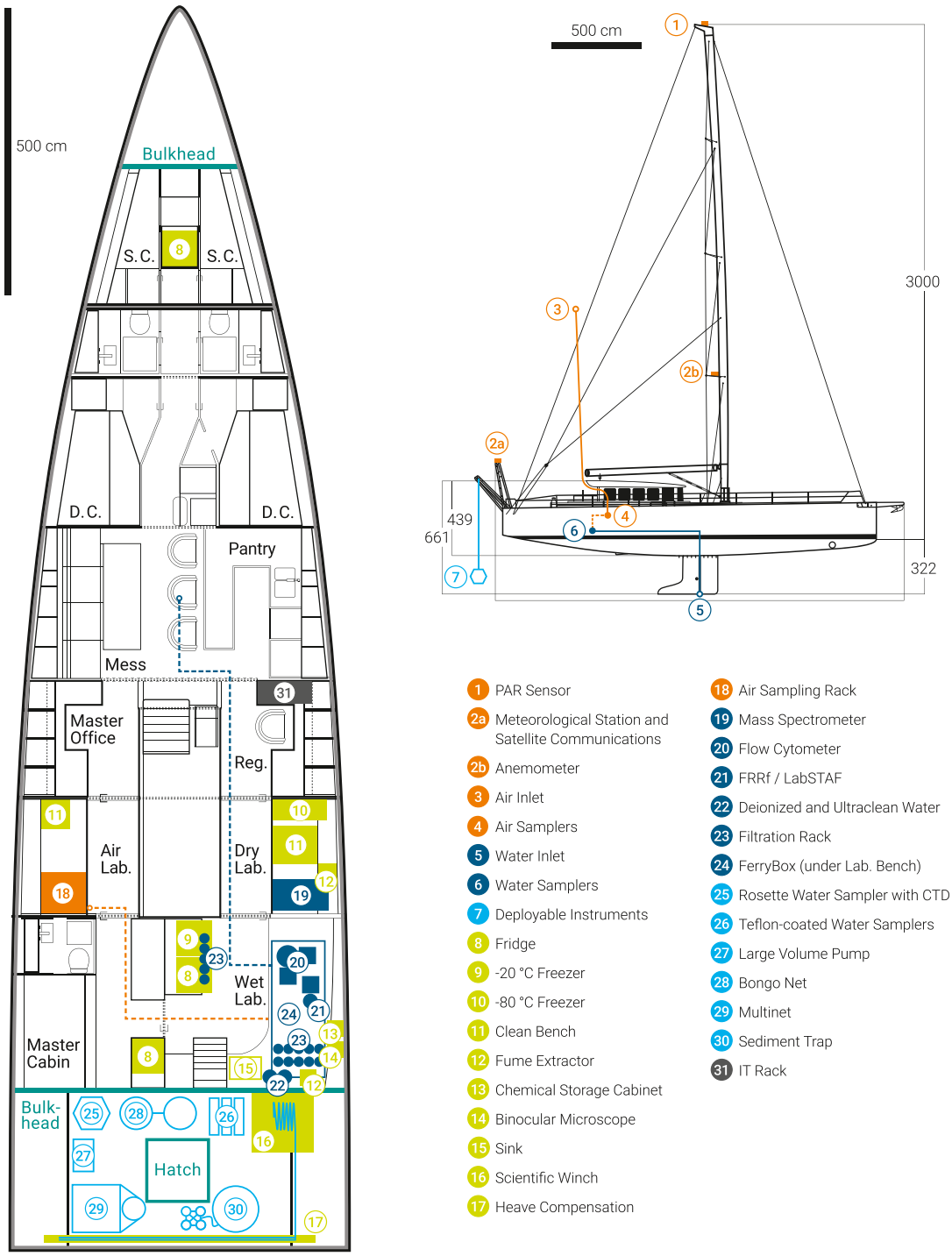

Figure 3. Layout of the *S/Y Eugen Seibold* (*ES*). Line drawing of side view (upper right panel), and layout of laboratories, storage room, and living quarters of the boat (left panel). Meteorological station, satellite communication systems, Photosynthetic Active Radiation sensor, and air sampling devices are shown in orange. Continuous sampling and analyses of seawater delivered from the keel inlet is shown in dark blue. Seawater sampling devices deployed over the A-frame at the stern of the boat are shown in light blue. Hatch of garage is shown in dark green. Scientific equipment is shown in light green. IT rack is shown in black. S.C. means single cabin, D.C. means double cabin, reg. is registration office. Dimensions (black numbers) are in centimeters. See Table 2 for explanation of the scientific probes. The *S/Y ES* has been assessed for safety according to the regulations of the ship's classification society, and is equipped with four life buoys, and two life rafts providing space for 12 people in total, that is, the maximum accommodation on single day cruises. Eight berths allow overnight accommodation. Bulkheads at the bow and stern provide safety buffer for collision and damage of the hull. The safety equipment such as EPIRB and survival suits are serviced and maintained by qualified companies. Laboratories and work areas are designed and assessed according to European and German national work safety regulations (DGUV 2020).

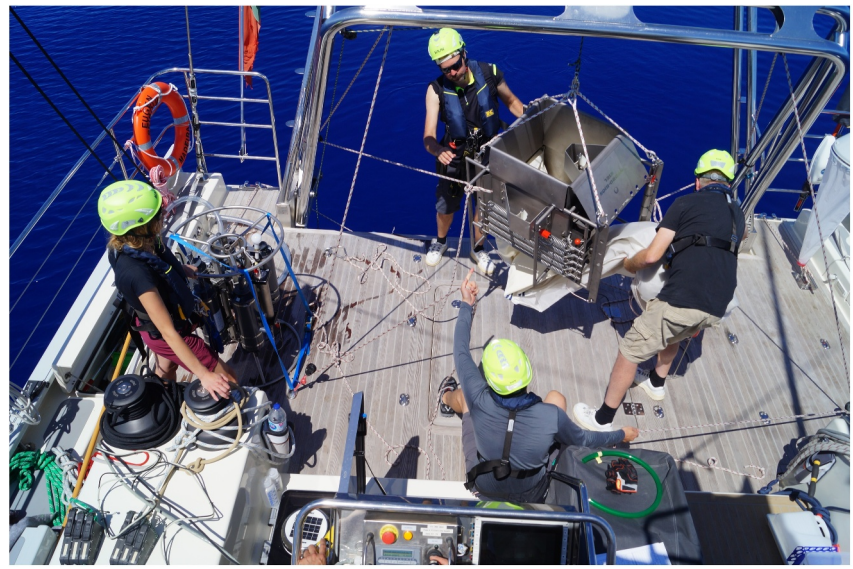

Figure 4. Work deck of the *S/Y Eugen Seibold* (*ES*). Deployment of the multinet (100-µm plankton nets) from the work deck of the *S/Y ES*. The rosette water sampler with five 5-L Niskin bottles is fixed at the starboard side of the work deck. The Apstein net for surface water phytoplankton sampling is fixed at the portside railing for drying. A-frame and winch are operated from the helmstand in the foreground. See Table 2 for the specifications of the devices. From the left to the right: Hedy Aardema, Hans Slagter, Jan Brüwer, Ralf Schiebel. Photo, M. Zahharov.

The air chemistry laboratory hosts a 19-inch instrument rack, a laboratory bench for sample preparation, and a laminar flow cabinet for contamination-free handling of samples (Table 2). The suite of aerosol instrumentation can be flexibly changed and adapted according to the scientific focus of the expeditions (Table 2). A low volume sampler with up to 24 filter holders (47 mm diameter) enables manual or automated filter sampling at pre-set intervals upstream of a cartridge housing as well as sampling semivolatile compounds on polyurethane foam (PUF), for simultaneous collection of particles and apolar organic trace gases, at flow rates of up to 50 L min^{-1} (Table 2). An Optical Particle Counter (OPC; Grimm Aerosol Technik, Ainring, Germany, The Dust Decoder, Model 11-D) for enumeration of aerosol particle number size distributions from 0.25 to 32 µm was installed in the air laboratory in 2022. A *Picarro* (Model G2508) gas concentration analyzer for quantification of gas concentrations of nitrous oxide (N_2O), methane (CH_4), carbon dioxide (CO_2), ammonia (NH_3), and water (H_2O), was installed in the air laboratory in 2022 (Busch & Busch, 1999).

A Coriolis μ air sampler installed on top of the wheel-house approximately 3.5 m above water line uses cyclonic impingement to collect particles into a liquid of choice with a sample air flow of up to 300 L min^{-1} (Table 2). This technique is primarily used for the collection of bioaerosols for subsequent analysis as it has been shown to minimize the physical stress on the cells collected, enabling downstream analysis of intact cells, as well as culture-based approaches (Dybwad et al., 2014).

Two aerosol microstations (*MICE@Sea*) equipped with optical particle counters, sensing in a range of 0.3–10 µm (5 bins), were installed in late 2022 on top of the wheel-house. Their performance and robustness in the marine environment are under evaluation in comparison to data from the other aerosol probes (Table 2).

Black carbon (BC, soot) particles are measured with a Single Particle Soot Photometer (SP2, Table 2) using laser-induced incandescence and scattering to determine the BC mass and mixing state of individual particles. As time resolution of SP2 data can be as high as 0.4 micro-seconds, the BC data obtained can also be combined with the wind data to help analyze the potential influence/contamination of the exhaust air of the *S/Y ES* on the air samples (Table 2).

2.4. BELUGA Eddy Tracker

BELUGA Navigator provides guidance for an adaptive sampling approach on *S/Y ES* expeditions, being linked with near real-time (Near Real-Time Transfer (NRT)) positions of the boat via satellite telemetry. Detection and

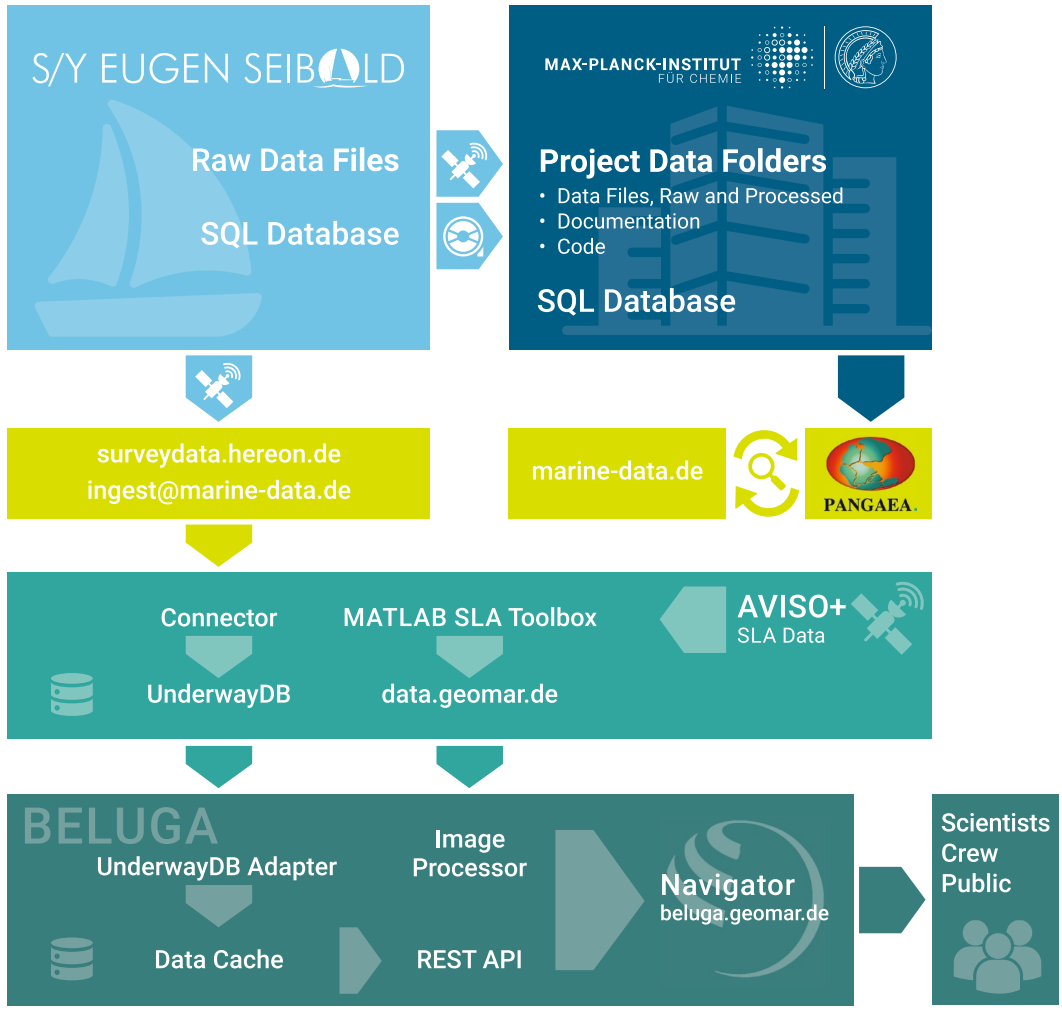

Figure 5. *S/Y Eugen Seibold* (*ES*) data flow. Raw data generated onboard include automated and manual logs produced on scientific events and other relevant activities such as emissions from the main engine or housekeeping (emission log). Some of the instruments send the data to a central Structured Query Language database onboard the *S/Y ES*, while others create raw data files, which are collected on a Network-Attached Storage. Near real-time (NRT Transfer) data flows of the expeditions, summarize connections between different data sources and involve processing steps of fed in data for final visualization via the *BELUGA Navigator*. The *BELUGA* Navigator visualizes locations of potential mesoscale eddy candidates derived from satellite sea level anomaly data together with the cruise track of *S/Y ES* (Leibold et al., 2023; https://beluga.geomar.de/eugen-seibold). REST API is Representational State Transfer Application Programming Interface.

tracking of mesoscale eddies in the Atlantic Ocean along route of the *S/Y ES* is performed by analyzing NRT sea level anomaly (SLA) satellite data distributed by AVISO (Archiving, Validation, and Interpretation of Satellite data). AVISO maps are automatically fed into the web-based application *BELUGA Navigator*, which has been developed at GEOMAR Helmholtz Center for Ocean Research Kiel (Figure 5).

BELUGA Navigator is the front-end component of the *BELUGA* system, which evolved from the *GEOMAR Navigator* project (Leibold & Al Abri, 2019), providing a standardized infrastructure for the aggregation of data from various marine measurement platforms, other observations such as remote sensing, and model data (Leibold et al., 2023). Originating from autonomous marine vehicles, *BELUGA* also offers capabilities for positioning and communication in underwater and surface networks, and allows interconnection with external data sources. Data transmitted by measurement platforms (e.g., position of *S/Y ES*) via satellite or other data links are imported into a central data back-end operated by GEOMAR's data management team. Integration of *S/Y ES* into *BELUGA* was realized by implementing a customized data importer to process vessel positions from a given internet resource

(Figure 5). Detection of potential eddy positions derived from SLA data was automatically performed on a daily basis by applying a vector-geometry eddy detection algorithm (Nencioli et al., 2010).

2.5. Meteorological Data

A *European Common Automated Weather Station* is installed on the A-frame at the stern of the *S/Y ES* by the German Weather Service (Deutscher Wetterdienst, DWD). Accordingly, the *S/Y ES* acts as a Voluntary Observing Ship as part of the Global Ocean Observing System, World Meteorological Organization (WMO), and Intergovernmental Oceanographic Commission. The weather data include data on air pressure, temperature, and RH, with, for example, 6,782 measurements from 1 January to 31 December 2021 (Der Wetterlotse, Maritime Meteo News, DWD). Navigational shipboard data are used for positioning of the weather data. Hourly weather reports are generated from the recorded data, and sent to DWD via an IRIDIUM Transceiver, and fed into the Global Telecommunication System of the WMO, for instantaneous weather forecasts and alerts, and various climatological applications. All of the data from the weather station are included in the general onboard scientific data collection.

2.6. Data Storage and Accessibility

Most measurement devices on the *S/Y ES* send the data instantaneously via the communication standard of the National Marine Electronics Association (*NMEA*). The *NMEA* messages are captured by custom-made software and stored in the onboard database. The current timestamp of the database server, which is synchronized with the onboard GPS-based time server, is saved with each data record. The GPS timestamp is stored as Coordinated Universal Time (UTC), and serves as a time reference for each metadata and measurement data point. This is of particular importance for the measuring devices, which cannot directly communicate with the onboard GPS-based time server. Synchronized timestamps in all data records facilitate full comparability of the data, and provide reliability when analyzing data sets of varying temporal resolution. The database also allows quick and easy access to the data for immediate evaluation of the data while measuring, and facilitates quality control and adjustment of sampling and recording strategies.

The onboard database server of the *S/Y ES* is capable of storing the data of the last three expeditions. The entire data set of all *S/Y ES* campaigns is stored on a central database server at the MPIC in Mainz. Data are transferred to Mainz online and via cartridges. A central mass storage device is available onboard for instruments, which produce large volumes of data, such as the *CytoSense* flow cytometer (Table 2).

3. Data Records

The Research Data Management of the *S/Y ES* has been designed to be flexible with respect to changes of the workflow and onboard technical setup, including changes in the format, storage, and transfer mode of raw data. The aim is to facilitate consistent publication of the resulting quality-controlled data (Figure 5) for all campaigns over the multiple projects and sampling seasons. Data acquisition on board is organized according to the logistical and technical constraints such as IT hardware capacity, limited satellite data transfer rates, and pre-defined file formats of the scientific instruments, to meet the requirements of the scientific work flow.

The published data are compliant with standards of the scientific community, to facilitate processing and exploitation of data to a maximum degree. Quality controlled data are published open access, some of them after a moratorium, according to the FAIR (Findable, Accessible, Interoperable, Reusable) principles (Wilkinson et al., 2016) at *PANGAEA*, www.pangaea.de (Felden et al., 2023).

In collaboration with *PANGAEA* and the project *DAM-Underway-Research Data* of the German Marine Research Alliance (Deutsche Allianz Meeresforschung, DAM), a processing and publication workflow has been developed (Figure 5). Expedition overviews including basic metadata and validated master tracks for each cruise are available from https://www.pangaea.de/expeditions/bybasis/Eugen%20Seibold (e.g., Walter et al., 2023). The master tracks have time resolutions of 10 s, and provide references for analyses of the scientific data.

A subset of data (e.g., temperature, wind speed, and sailing direction) are instantly sent with reduced time resolution as NRT via satellite to HEREON (Geesthacht, Germany), from where they can be accessed as open access data via the portal *surveydata.hereon.de* (Figure 5). Another NRT branch to the Alfred Wegener Institute (AWI, Bremerhaven) allows access to additional parameters for scientists involved in the project, by sending emails to

ingest@marine-data.de (Figure 5). Both NRT branches are supported by the *DAM-Underway-Research Data* partners. In addition, daily data packages are sent to MPIC via File Transfer Protocol.

With respect to the data volume, only a small fraction of the data is transferred at sea via satellite so far. When back in port, the MPIC instance of the Structured Query Language database is fed with new data from the onboard database, and the files of the Network-Attached Storage are transported via cartridge to the MPIC. At MPIC, the files are checked for duplicates and sorted into a structured project data folder on the MPIC file server. The project folder contains raw data (level "L_0") and processed data (levels L_2, L_3, and L_4 for original resolution, averaged data, and merged data compilations, respectively). Intermediate steps (L_1) are kept if required. In addition, metadata, descriptions of the parameters, and further documentation are placed on the data server. The project folder also contains data from the laboratory analyses of discrete samples, *in-progress* summary tables for daily use, technical and organizational notes, supplementary data (e.g., from satellites, models), and other files of temporal relevance. In addition to the digital logs, log sheets are filled for each deployment of a sampling device, recording metadata such as type of device, position, date, and time, data on weather (e.g., wind and cloud cover) and sea state (e.g., swell and wave height), as well as information on the samples (sampling depths, volume of water filtered or sampled).

Labels identify each campaign, station, cast, and event with a consistent syntax of the format:

- Campaign labels: ESyyC**cr**, for example, *ES20C04*: ES, 2-digit year (e.g., 20), 2-digit cruise (e.g., 04)
- Station labels: ESyyCcr_**sta** with three digit station number, for example, *ES20C04_017*
- Cast labels: ESyyCcr_sta_**ca** with two digits, for example, *ES20C04_017_03*
- Water sample labels: ESyyCcr_sta_ca_**sa**_prop with two digit-bottle number and the sample type or property. For example, a water sample from the Cruise 04 in 2020, Station 017, Cast 03 with the rosette water sampler, Niskin bottle 06, and sampled for nutrient analysis, would have the label *ES20C04_017_03_06_nuts* (i.e., nutrients). The prefix *SYES* (*for S/Y ES*) is added to each event label, for example, *SYES_ES19C01*, to guarantee unique labels within the *PANGAEA* repository.

For sharing data with the scientific community and ensuring long-term accessibility, the processed data are published in an interoperable way as relational data sets in the open access *PANGAEA* repository, where the data can be visualized in the web browser, or downloaded as tab-separated data files. *PANGAEA* offers web services and a data warehouse for searching and retrieving data, and data access by the programming languages Python and R. Metadata are essential for the reusability of the data. Each relational data set in *PANGAEA* contains basic metadata such as information on authors, as well as title, abstract, and description of the individual parameters. Further details are given by links to standard operating procedures, data processing reports, and the code used for data processing.

To enhance findability of the marine research data, the data portal *marine-data.de* has been established by *DAM-Underway-Research Data*. In this portal, a growing number of (German) research vessels including the *S/Y ES* have their own subpage, which serves as a starting point for browsing and searching data, showing a map with the ship track and available parameters, and providing the links to the corresponding data sets stored in *PANGAEA* (Felden et al., 2023).

4. Data and Samples Obtained Along the 20-West-Transect

The *S/Y ES* expeditions sampled a meridional transect along 20°W in the North Atlantic from 2019 to 2021, including eight marine provinces (Figure 2) of the subpolar to tropical NE Atlantic representative of most of the global marine biomes and climato-genomic provinces (Frémont et al., 2022; Longhurst, 2007; Reygondeau & Dunn, 2019; Sutton et al., 2017). The water column was sampled to a maximum water depth of 700 m at nine stations (Figure 2). The so-called ESTOC* station at 29.5°N 15°W, near the European Station for Time-Series in the Ocean Canary Islands (ESTOC, 29°N 15°W), was sampled repeatedly (Table 3). In total, 1,223 underway samples from 3 m water depth, and 182 air samples including aerosol samples (Table 2, Bioaerosol and Low Volume Filter Samplers), were collected (Table 3). From the surface and subsurface water column, 1,802 samples were obtained with the water sampler, large volume pump, and plankton nets (Table 2). The metadata on the campaigns, stations, casts, and events are available from *PANGAEA* at https://www.pangaea.de/expeditions/bybasis/Eugen%20Seibold (e.g., Walter et al., 2023). All data presented in this paper have been published in the *Edmond Open Research Data Repository* of the Max Planck Society (Schiebel, 2024).

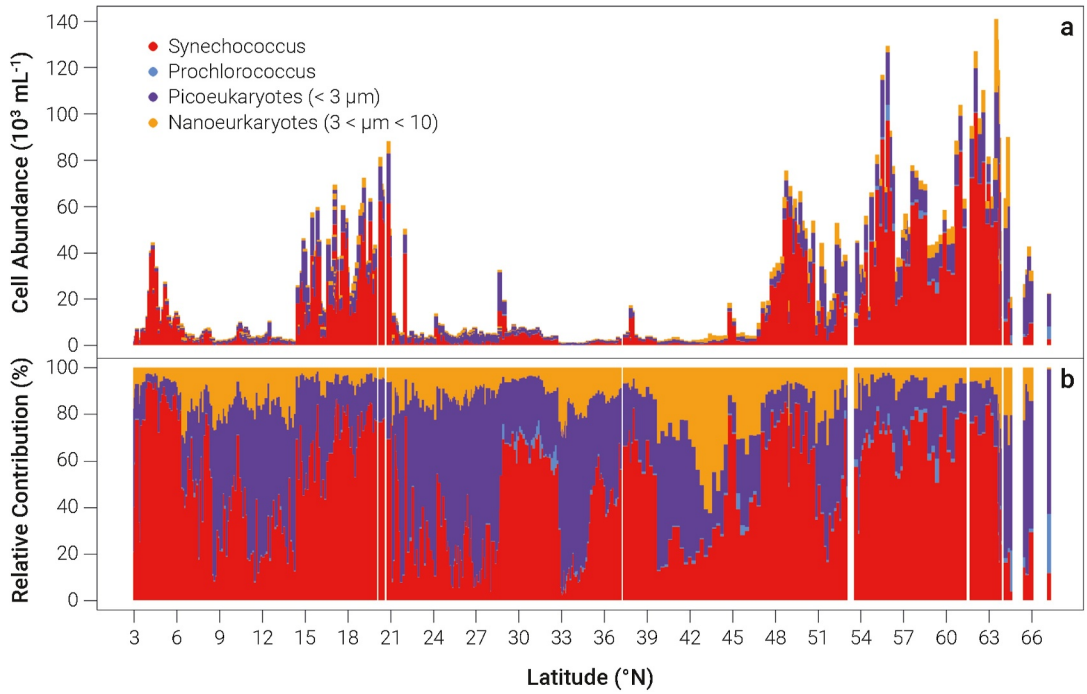

Figure 6. Underway flow cytometry data on pico- and nano-phytoplankton at 3 m water depth. (a) Absolute cell numbers (top panel) and (b) relative abundance (bottom panel) of different phytoplankton groups by size and pigment composition, derived from flow cytometry. Cyanobacterial groups, separated by cells size and fluorescence at 631 nm (red spectrum, representing Phycobilin), include predominantly *Synechococcus* and *Prochlorococcus*. Eukaryotic phytoplankton are classified by size and fluorescence at 684 nm (red spectrum, representing chlorophyll). The horizontal axis represents the latitude from the equatorial waters to the polar circle.

Quality-controlled data from the lower atmosphere and surface ocean are presented to embrace the range of joint and multi-facetted scientific approaches combined within the *S/Y ES* project, and facilitate maximum scientific gain for an improved understanding of the climate related biogeochemical exchange processes between the atmosphere and ocean. Data on stable isotopes and cation-to-calcium ratios from ambient seawater and planktic archives (foraminifers) produced in conjunction with full suite of environmental parameters are meant to provide a glance at the paleo-perspective of the project.

4.1. Phytoplankton as Basis of the Marine Food Web

Phytoplankton are unicellular photosynthetic organisms and one of Earth's major sources of oxygen, and consumers of atmospheric CO_2, while forming the basis of the marine food web (Field et al., 1998). Being about 0.6 and 0.9 µm in size, the marine cyanobacteria *Prochlorococcus* and *Synechococcus*, respectively, dominate the open ocean phytoplankton, and are possibly the most and second most abundant photosynthetic organisms on Earth (Partensky et al., 1999). As planktic organisms have little to no control over their position in the water column, they depend on the physical and chemical state of ambient seawater. As phytoplankton are the first and foremost interacting organisms in the food web, their nutrient uptake, metabolic products, and organic remains strongly affect the physico-chemical state of the surface to deep ocean via dissolved and particulate matter fluxes (Koeve & Ducklow, 2001). Finally, changes in Earth and ocean climate are expected to result in diverse changes in phytoplankton abundance and composition, and thus chemical state of the oceans, such as carbon cycling (Behrenfeld et al., 2006; Brun et al., 2019; Huisman et al., 2006; van de Poll et al., 2013).

Picophytoplankton (<3 µm; Vaulot et al., 2008) and nanophytoplankton (3–20 µm) were quantified by flow cytometry (Table 2) and separated from photoautotrophic prokaryotes by fluorescence of their photosynthetic pigments (Figures 6 and 7). Samples were taken from the keel inlet every 1–2 hr, resulting in an average spatial resolution of 6–16 nautical miles, along the 20°W transect between 67°N and 3°N (Figure 2). In addition, vertical profiles spanning the photic layer were enumerated from discrete samples at eight stations on Expeditions

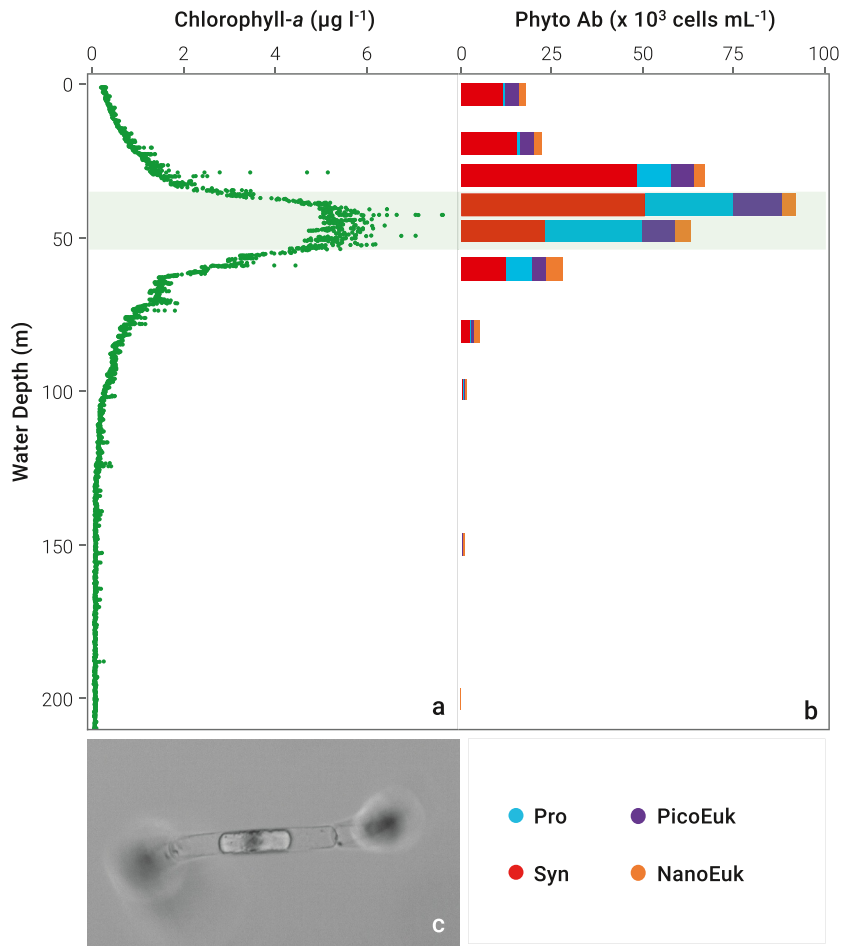

Figure 7. Data on chlorophyll-*a* fluorescence and flow cytometry of the pico- and nano-phytoplankton from the upper water column. (a) Vertical profiles of chl-*a* fluorescence over the epipelagic layer at Station19 between Ireland and the Azores (Figure 2). Light green bar represents the Deep Chlorophyll Maximum (DCM) between 40 and 50 m water depth. (b) Vertical abundance of different phytoplankton groups counted by flow cytometry on board. Depths scales of the panels (a) and (b) are the same. Bars show abundances of the four major phytoplankton groups (Phyto Ab), *Prochlorococcus* (Pro, blue), *Synechococcus* (Syn, red) Pico-Eukaryotes (PicoEuk, purple), and Nano-Eukaryotes (NanoEuk, orange) at all sampled depths (3, 20, 30, 40, 45, 60, 80, 100, 150, and 200 m). Cell numbers display an absolute maximum and an increase in diversity at the DCM. The small phytoplankton cells dominate the NE Atlantic autotrophic biomass, and are predicted to increase with stratification caused by climate warming. (c) Image of a diatom acquired with the *CytoSense* at surface waters in the Madeira Basin (Figure 2, C09).

ES20C04 to ES21C16 (Table 3). Seasonally distinct communities are observed and support interpretation of the physical, chemical, and biological processes in the upper ocean and lower atmosphere.

Overall, phytoplankton were alternatingly dominated by cyanobacteria and eukaryotic picophytoplankton, and nanophytoplankton was present at subordinate abundances. Total abundances varied by two orders of magnitude between regions of contrasting trophic conditions (Figures 2 and 6). The northernmost, subpolar latitudes show typical high primary productivity with highly diverse communities (Figure 6), being delineated from the seasonally less productive temperate ocean by a hydrologic front along the northern branch of the Gulf Stream called the North Atlantic Current at roughly 47°N (Figures 2 and 6). Between 21°N and 14°N, the *20-West-Transect* intersects the productive Mauritanian coastal upwelling region from which filaments and mesoscale eddies propagate westward. An eddy with enhanced primary productivity associated with Equatorial upwelling was sampled between 3°N and 6°N (Figure 6).

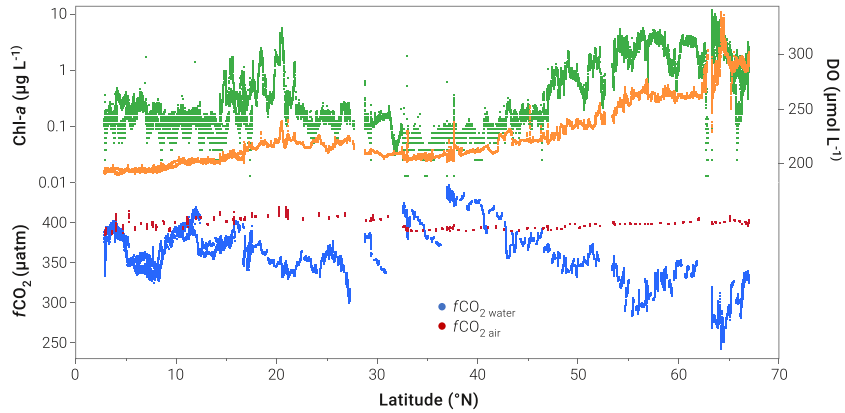

Figure 8. Comparison of underway CO_2, chlorophyll-*a*, and dissolved oxygen (DO) concentration measured at 3 m water depth. Progression of latitudinal changes in chl-*a* fluorescence (logarithmic scale, µg L^{-1}, green), DO (µg L^{-1}, orange), and CO_2 fugacity (fCO_2, µatm) in the surface water (blue) and the lower atmosphere (red), between 67°N and 3°N latitude in the eastern North Atlantic.

Less productive waters with total phytoplankton abundances below 20×10^3 cells mL^{-1} showed alternating relative abundances between prokaryote and the smallest eukaryote phytoplankton (Figure 6). Total phytoplankton abundances increased by up to two orders of magnitude from the surface mixed layer to the Deep Chlorophyll Maximum (DCM) in particular in strongly stratified oligotrophic regions, along with changes in the relative abundance of different size groups (Figure 7). Such changes in the relative contribution of the pico- and nano-phytoplankton groups were spatially often connected, and temporally succinct (Figure 6). This implies seasonal effects, which may be elucidated by a more complete seasonal coverage via sampling on future expeditions.

Low numbers of *Prochlorococcus* (Figures 6 and 7) may result from underestimation of the cells counts by the *CytoSense* (Table 2). The small size and limited photosynthetic pigment content of *Prochlorococcus* display a dim fluorescent signature, particularly when exposed to high light intensities in surface waters, generating a signal very close to the limit of detection capacity of the *CytoSense* (Marrec et al., 2018). The discrepancy between real and *CytoSense*-detected numbers of *Prochlorococcus* is possibly largest in subtropical oligotrophic waters where higher numbers would be expected (Buitenhuis et al., 2012).

4.2. Biologically Active Gases

The combination of high spatial and temporal resolution sampling of biologically active gases with microbial communities, and detailed environmental and geochemical data facilitate a better understanding of the role of marine microbes in the uptake of CO_2 (sink capacity) of the oceans and impacts on global climate change. Despite their importance for ocean productivity and atmospheric particle (incl. aerosol) turnover, latitudinal gradients of microbial ecosystem functioning, effects on the air-sea exchange of CO_2, and aerosol formation are still not well understood. Unprecedented high spatial and temporal resolution of the samples obtained with *S/Y ES* allow for computation of these dynamics at the scale of the relevant key processes (i.e., at the range of kilometers and minutes), and facilitates a better understanding of marine microbial communities, ocean productivity, and air-sea CO_2 exchange (Figures 6, 8, and 9), which play a pivotal role in ocean carbon sequestration and climate change.

The high-resolution data of both surface water (from ca. 3 m water depth) and atmospheric (13 m above sea surface) CO_2 fugacity cover a wide range of productivity regimes as evidenced by changes observed in chl-*a* fluorescence along the latitudinal transect. Whereas biological productivity causes changes in CO_2 and dissolved oxygen (DO; Figure 8), the effect of seasonal variability, together with solubility changes due to latitudinal gradients in salinity and temperature (Figure 2) still needs to be analyzed in detail. Higher concentrations of chl-*a* at northern latitudes (July 2020) indicate more productive cold waters (Figures 2 and 8), with low surface water CO_2 values and enhanced DO concentration due to high microbial photosynthetic rates (Figure 9). This region acts as a sink for atmospheric CO_2. In contrast, at tropical and subtropical latitudes (April and May 2021), warm waters show lower chl-*a* fluorescence, implying less productive and more oligotrophic conditions with surface water CO_2 values closer to and eventually surpassing atmospheric CO_2 (between 35°N and 40°N), which can

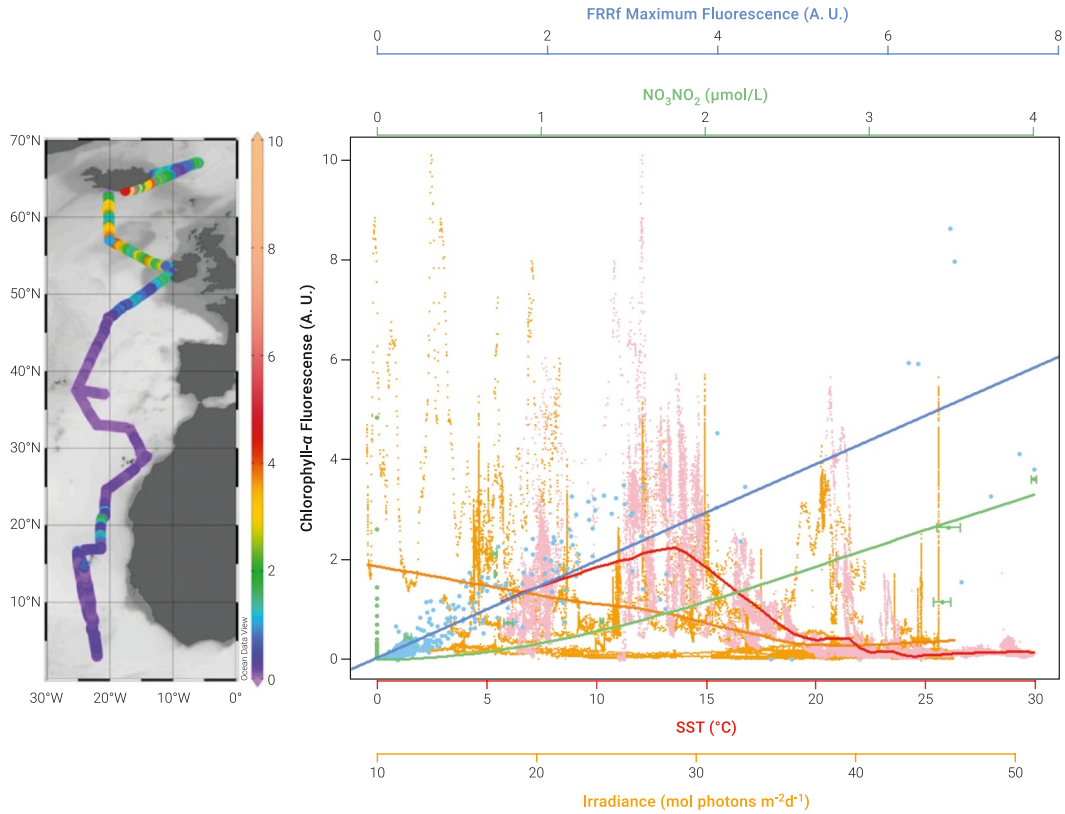

Figure 9. Covariation of environmental variables with chlorophyll-*a* fluorescence. Chlorophyll-*a* fluorescence (a.u.) from the polar circle near 67°N to the equatorial upwelling at 3°N given as color gradient in the left panel, and in the right panel against sea surface temperature (SST, red), irradiance at the sea surface (in mol photons m^{-2} d^{-1} corrected for reflection, orange), NO_3NO_2 concentration (µmol L^{-1}, green), and dark-regulated Fast Repetition Rate (FRR) maximum fluorescence (a.u., blue). Data points correspond to individual measurements while the lines are fitted using a linear model (FRR minimum fluorescence) or a LOESS fit (SST, I_{ML}, and NO_3NO_2). The chl-*a* fluorescence was measured using an ECOtriplet fluorometer (ex/em 470/695 nm) mounted in the *FerryBox*.

result in the ocean performing as a moderate regional source of CO_2 to the atmosphere (Figure 8). An exception is the West African upwelling region between 14°N and 25°N (April 2021), evidenced by changes in phytoplankton abundance and chl-*a* (Figures 6 and 8, respectively), where increased phytoplankton biomass is triggered by nutrient enriched waters. The consequent biological drawdown of CO_2 in surface waters counterbalanced the physical CO_2 supply from subsurface waters has been often observed in the coastal upwelling off the northwest African coast (Lefèvre et al., 2023).

Overall, our data show that the variability of biological properties (e.g., chl-*a* concentration and phytoplankton cell abundance) sampled along the latitudinal transect exert a control on surface dissolved gases (both CO_2 and O_2), regardless of the productivity regime and the physico-chemical characteristics of the waters sampled (e.g., temperature and salinity). The separated effects of biological activity, seasonal variability and changes in solubility due to salinity and temperature variability are being analyzed in detail.

4.3. Phytoplankton Photosynthesis

To optimize growth, phytoplankton use a wide range of both long and short-term adaptive responses to variable light conditions. How the phytoplankton community can adapt to light conditions is dependent on environmental conditions such as temperature and nutrient concentrations (Figure 9), and the phytoplankton community composition (Behrenfeld et al., 2006; Suggett et al., 2009). The attained growth efficiency drives primary productivity and many biogeochemical cycles (Gorbunov & Falkowski, 2022). Complementary data on biological processes in the surface ocean is provided by multiple automated and synchronized sensors in the wet and dry

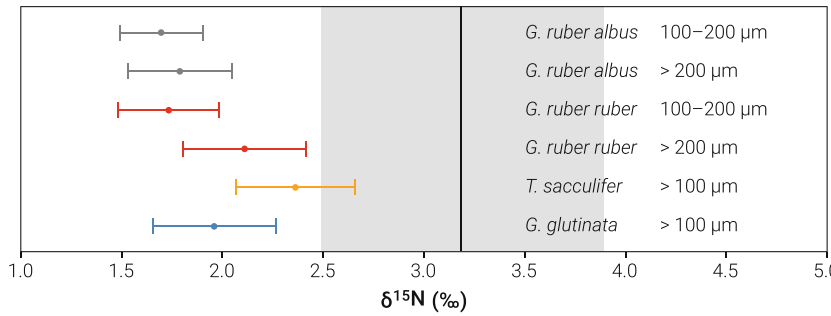

Figure 10. $\delta^{15}N$ of different planktic foraminifer species and size classes provide differential information on ecological conditions. Whereas *Globigerinita glutinata* is barren of photo-symbionts, *Globigerinoides ruber* of both chromotypes white and red (*G. ruber albus* and *G. ruber ruber*, respectively) and *Trilobatus sacculifer* harbor dinoflagellate algae as photo-symbionts, which lowers the $\delta^{15}N$ of the foraminifer shells, that is, higher $\delta^{15}N$ at lower symbiont activity (Smart et al., 2018). In addition, higher $\delta^{15}N$ can indicate a more carnivorous diet, and lower $\delta^{15}N$ a more herbivorous diet. The respective standard deviations and standard errors are indicated by the error bars (Bieler, 2022). Gray line and shading show arithmetic mean and standard deviation (1SD) of $\delta^{15}N$ of the regional subsurface waters (Fripiat et al., 2021).

laboratories (Figure 3). The combination of an *ECOtriplet* fluorometer with chlorophyll and phycocyanin fluorescence channels, an oxygen optode, pCO_2 analyzer, fluorometer (*FRRf*), flow cytometer, and Membrane Inlet Mass spectrometer (Table 2) provide a unique set of data on marine photosynthesis and primary productivity. Discrete samples for chlorophyll concentration, light microscopy, spectral absorption (QFT), and DNA sequencing provide additional information on the phytoplankton community. During the S/Y *ES* cruises in 2020 and 2021 (Table 1), these methods were applied concurrently to sampling of a multitude of environmental variables affecting phytoplankton photosynthesis (Figure 9).

The *20-West-Transect* crossed a wide range of chlorophyll concentrations with a general trend of high chlorophyll fluorescence at higher latitudes and local spatial variability such as the increase in fluorescence caused by upwelling off the coast of Mauritania around 21°N 21°W (Figure 9, left panel). An exploratory plot of the covariation of environmental variables with chl-*a* fluorescence shows the complexity of these relationships (Figure 9, right panel), such as peak chl-*a* fluorescence at sea surface temperatures between 10 and 15°C, and an opposing trend of irradiance (mol photons m^{-2} d^{-1}) at the sea surface in relation to an overall effect of nutrient limitation. The high spatial resolution of the underway measurements in combination with the vertical profiles in distinct ocean regions will allow for further unraveling the variability of phytoplankton photophysiology and productivity at the regional scale (Aardema et al., 2024).

4.4. Calcareous Plankton as an Archive of Climate Change

Calcareous plankton are analyzed and calibrated by using the physical, chemical, and biological data obtained along with the respective plankton net samples (Table 2). Planktic foraminifers are the most frequently used carriers of proxies in the reconstruction of past conditions in the ocean and overlying atmosphere (e.g., de Garidel-Thoron et al., 2022; G. Fischer and Wefer, 1999; Kucera, 2007; Schiebel & Hemleben, 2017; Vincent & Berger, 1981). Most calibration work has so far relied on the foraminifer tests that have recently accumulated on the seafloor (e.g., CLIMAP, 1981; Siccha & Kucera, 2017). This is an efficient approach because the sediments are a natural concentrator of foraminifer tests relative to the other components of upper ocean biomass, but they also integrate over large-scale spatial patterns (e.g., Siegel & Deuser, 1997) and long-term (decades to millennia) open marine processes (Völker et al., 1998). Collection of living foraminifers, in contrast, allows many additional aspects to be investigated, including depth habitat, seasonality, ontogeny, interannual variability (e.g., Schiebel & Hemleben, 2000), and various proxies of their organic tissue and shell for paleoceanography and paleoclimate reconstruction (Figure 10).

4.4.1. Nitrogen Isotopes of Marine Plankton

Nitrogen (N) and phosphorus (P) limit biological productivity throughout most of the tropical to temperate oceans. Both the cycling of N and its input/output budget control the fertility of the ocean, and play a key role in

setting the concentration of atmospheric CO_2 (D. M. Sigman & Haug, 2003). The two stable isotopes of N, ^{14}N, and ^{15}N represent a powerful tool to quantify changes in the marine N cycle in present and past oceans (Deutsch et al., 2004; D. M. Sigman et al., 2009).

Depending on the environmental settings, changes in N isotopic signatures can reflect processes such as the degree of nitrate consumption in the surface ocean, N_2 fixation, or water column denitrification (D. M. Sigman et al., 2009). N isotopic signatures are incorporated by organisms into newly formed biomass and some fraction is ultimately transported to the seafloor and accumulated in the sediment (Altabet et al., 1999; Thunell et al., 2004). However, the $\delta^{15}N$ signature produced in the surface ocean may be either altered during sedimentation, or contaminated with allochthonous N, for example, from terrestrial sources (Altabet & Francois, 1994; Robinson et al., 2012; O. M. Sigman et al., 1999).

Ground-truthing and calibration of both foraminifer and diatom-bound $\delta^{15}N$ is a major step in proxy development for paleoceanographic application of fossil-bound $\delta^{15}N$. Sampling oceanic transects across a wide range of trophic conditions is key to facilitate a complete interpretation of the fossil-bound N isotopes (Auderset et al., 2022; Schiebel et al., 2018; Smart et al., 2018, 2020). The *S/Y ES* contributes to this effort by employing net tow sampling and high-volume filtration (Table 2), to collect foraminifers and diatoms, respectively. Plankton samples and data obtained with the *S/Y ES* allow for establishing the relationship of foraminiferal biomass to shell-bound $\delta^{15}N$ for different species, including intra-species differences in the $\delta^{15}N$ over the seasonal development, and comparison of the foraminiferal isotope data with the surface-ocean N pools (Bieler, 2022; Ren et al., 2009; Schiebel & Movellan, 2012; Smart et al., 2018, 2020). Environmental parameters recorded and sampled in parallel to the foraminifers yield empirical relationships for a mechanistic understanding of foraminifer-bound $\delta^{15}N$ in the open ocean (Table 2).

For example, planktic foraminifers sampled with a net tow (Table 2) from the surface water column of the oligotrophic subtropical gyre of the North Atlantic near the Canary Islands (Figure 2) in May, show varying cell tissue N isotope signals of the surface-dwelling symbiont bearing species (Bieler, 2022), which are lower than the $\delta^{15}N$ of nitrate supplied to the mixed layer from subsurface waters (Figure 10) (Fripiat et al., 2021). The relatively low $\delta^{15}N$ observed in the subsurface can be the result of N_2 fixation (Bieler, 2022). Any size-dependent differences in $\delta^{15}N$ of the same species (Figure 10) may facilitate a more detailed comprehension of the marine nitrogen cycle and surface ocean ecosystem structure of modern and past oceans (Bieler, 2022).

4.4.2. Mg/Ca in Planktic Foraminifers as a Temperature Proxy

The ratio between magnesium and calcium (Mg/Ca) of foraminiferal test carbonate is a ubiquitous proxy in paleoceanography that merits improvement. Regional rather than global calibrations are needed for a detailed systematic comprehension of the marine environment and climate geochemistry. The Mg/Ca of different planktic foraminifer species potentially provides temperature reconstructions of the surface mixed layer, the underlying thermocline, and the sub-thermocline water body (Elderfield et al., 2002; Friedrich et al., 2012; Nürnberg et al., 1996). Exponential relationships of foraminiferal Mg/Ca to ambient seawater temperature (i.e., calcification temperature derived from $\delta^{18}O$) in sediment trap, seafloor sediment samples, and culture studies have demonstrated the robustness of this geochemical paleothermometer. However, none of these approaches entirely captures the environment in the upper hundred meters of the ocean water column in which planktic foraminifers live and calcify their shells. With each of the so far employed approaches, calcification temperature estimates are being based on $\delta^{18}O$ assuming isotopic equilibrium. Culture studies circumvent these uncertainties, but provide data on an artificial environment, which does not fully capture the natural conditions. Therefore, in situ calibration studies of the Mg/Ca paleothermometer in the modern ocean may significantly contribute to improve the accuracy and interpretation of past SST reconstructions (A. Fischer et al., 2024).

In addition to species- and size-specific calibrations, Jochum et al. (2019) showed significant chamber-to-chamber variation of Mg/Ca in applying femtosecond laser ablation inductively coupled plasma mass spectrometry (fs-LA-ICP-MS) to planktic (and benthic) foraminifers, and suggest not to use the final chamber for Mg/Ca paleo-thermometry. Accordingly, analyzing the penultimate (Equation 1; Line 7 in Figure 11) and antepenultimate (Equation 2; Line 8 in Figure 11) chambers of *G. ruber albus*, a Mg/Ca temperature relationship for the subtropical North Atlantic (Madeira Basin; Figure 2) is proposed (A. Fischer et al., 2024). Chamber specific equations are selected on the basis of highest correlation with equations provided in the literature (Figure 11). The resulting generalized temperature relationship for the penultimate and antepenultimate chambers are given as

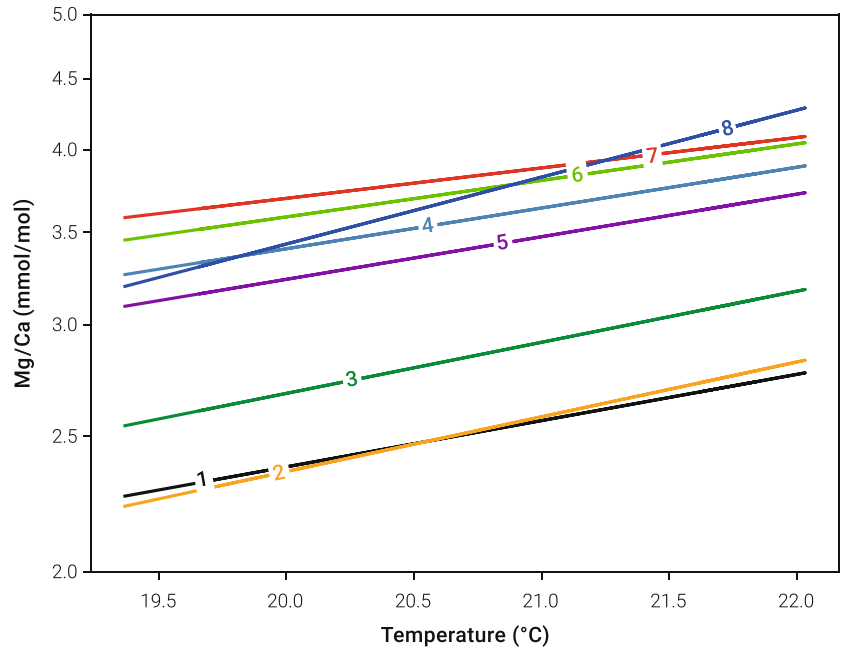

Figure 11. Mg/Ca paleo-thermometry calculation. Comparison of published (1–6) Mg/Ca paleo-thermometers for *G. ruber* with the two Mg/Ca thermometers derived from the penultimate (7) and antepenultimate (8) chamber of *G. ruber albus* relative to ambient water temperature, that is, sea surface temperature, SST (A. Fischer et al., 2024). Colored lines and numbers refer to (1) Sadekov et al. (2009), (2) Anand et al. (2003), (3) Mohtadi et al. (2009), (4) Bolton et al. (2011; penultimate chamber, F-1), (5) Bolton et al. (2011, antepenultimate chamber, F-2), (6), Gray et al. (2018). Please note the logarithmic (ln) scale of the *y*-axis.

$$\mathrm{Mg/Ca} = 1.36\ (\pm 0.66)\ e^{(0.05(\pm 0{:}02)T)} \quad (1)$$

$$\mathrm{Mg/Ca} = 0.38\ (\pm 0.30)\ e^{(0.10(\pm 0.04)T)} \quad (2)$$

4.4.3. Oxygen and Carbon Isotopes of Planktic Foraminifer Tests and Ambient Seawater

Oxygen ($\delta^{18}O$) and carbon ($\delta^{13}C$) isotopes are the most ubiquitous proxies in paleoceanography both of which are retrieved in a single measurement. While the oxygen isotopes have often been the goal of the analyses, the carbon isotope data are frequently not even reported because there is great uncertainty and controversy in how these data should be interpreted, resulting from the numerous factors (e.g., varying $\delta^{13}C$ sources, foraminifer respiration, photo-symbiont activity) that can affect the $\delta^{13}C$ signal (e.g., Spero & Williams, 1988). An adequate calibration of foraminifer shell $\delta^{13}C$ that embraces the complexity of this proxy and attempt to deconvolve the multiple proposed effects would make this proxy useable and provide access to one of the world's largest paleoceanographic data sets (Mulitza et al., 2022), years or decades after it was generated.

For foraminiferal $\delta^{13}C$ proxy calibration, data on the isotope composition of the DIC pool used by the foraminifers to grow their tests are of pivotal importance. The isotope composition of the DIC pool is strongly affected by primary productivity, and can therefore be highly variable along depth profiles and between seasons. Precise assignment of the corresponding DIC $\delta^{13}C$ values to the water depth of calcification of planktic foraminifer tests would significantly reduce the uncertainties in our understanding of how foraminifers capture carbon from seawater.

$\delta^{13}C$ DIC data of the water column between 3 and 450 m water depth at the Cape Verde Ocean Observatory, in the subtropical eastern North Atlantic (Station 29, Table 3), display a typical vertical covariation of DIC $\delta^{13}C$ and different measures of primary productivity (Figure 12). In combination with plankton tow samples of planktic foraminifer tests, these data facilitate assignment of proper $\delta^{13}C$-DIC values from specific sampling depths and times for a better understanding of the existing and new data sets of foraminiferal $\delta^{13}C$ values as a proxy of paleo-

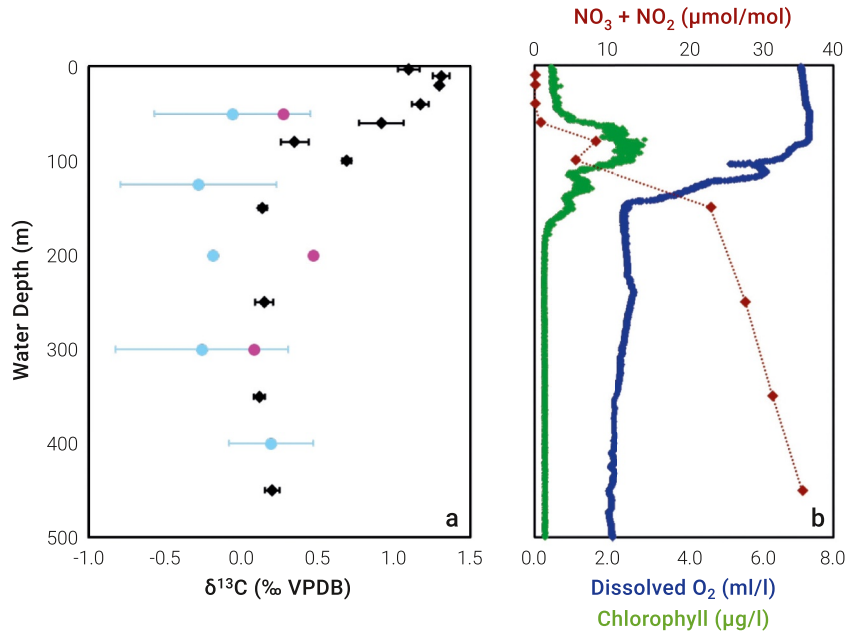

Figure 12. Dissolved inorganic carbon $\delta^{13}C$ as proxy of past ocean primary productivity. (a) Covariation of $\delta^{13}C$-DIC (black diamonds) with (b) chlorophyll-*a* fluorescence (green line) with a maximum around the deep chlorophyll maximum, and dissolved oxygen (blue line) as measures (from CTD75M; Table 2) of primary productivity in the eastern subtropical Atlantic northeast of São Vicente, Cape Verde (Station 29, Figure 2). $NO_3 + NO_2$ data (red diamonds) were measured on discrete seawater samples at the MPIC, Mainz. (a) $\delta^{13}C$ of the calcareous tests of the two planktic foraminifer species *G. ruber albus* (light blue dots) and *G. ruber ruber* (pink dots) show a systematic offset for the $\delta^{13}C$-DIC of ambient seawater (black dots), and may be applied as proxies of past ocean and climate changes.

productivity in the subtropical oceans. As the $\delta^{13}C$ values of the planktic foraminifer shell calcite are closer to the $\delta^{13}C$-DIC values of the thermocline and sub-thermocline waters (0‰–0.5‰VPDB) than surface values (>0.8‰), they may not display the trophic conditions of ambient sea water they were sampled from. With an average life span of a fortnight, the surface-dwelling species *G. ruber albus* may have formed their test calcite closer to the thermocline and DCM as the main food source, or in adjacent upwelled water bodies over the days and weeks preceding the sampling (Schiebel & Hemleben, 2017). The systematically higher $\delta^{13}C$ of *G. ruber ruber* than *G. ruber albus* (Figure 12) are close to the surface $\delta^{13}C$-DIC, and may not be related to any earlier upwelling, indicate conditions closer to the ambient water body at the time of sampling. Additional data on a larger spectrum of ecological conditions in other regions of the oceans are needed to provide a better understanding of the different $\delta^{13}C$ pools, varying trophic conditions of the oceans, and their effect on the air-seawater greenhouse gas exchange and paleoclimate.

4.5. Atmospheric Aerosols and Composition of Microbial Communities in Ocean Air and Surface Waters

Atmospheric aerosols consist of airborne solid and liquid particles in the nanometer to micrometer size range, which play a fundamental role in the Earth climate system by influencing the radiative balance of the atmosphere, the formation and development of clouds and precipitation, and the airborne spread of organisms and diseases (Fröhlich-Nowoisky et al., 2016; Pöschl, 2005; Ramanathan et al., 2001). Aerosol particles serving as cloud condensation nuclei or ice nuclei (IN) affect the microphysical processes and dynamic evolution of clouds (Brooks & Thornton, 2018). A comprehensive understanding and correct representation of marine cloud dynamics, lifetime, and reflectivity are essential for global climate modeling, since the oceans account for more than 70% of the Earth's surface, and their cloud coverage affects the Earth's radiative balance. Furthermore, atmospheric aerosols affect the biogeochemistry of the ocean-atmosphere exchange through the deposition of micronutrients to the phytoplankton as the base of the marine food web (Hamilton et al., 2022).

The marine aerosol is characterized by a high spatiotemporal variability as well as diverse chemical composition and complex physicochemical properties (Heintzenberg et al., 2000). It represents a mixture of natural and

anthropogenic emissions derived from both continental and oceanic sources. The atmospheric residence times of aerosol particles typically range from days to weeks. Continental aerosols from fossil fuel or biomass combustion, smoke, dust, and biogenic particles from the continental biosphere can be transported over long distances and may reach remote regions of the oceans. Pristine states of the marine atmosphere are of particular relevance to understand and model the extent of anthropogenic perturbations of the present-day and future atmosphere (Andreae, 2007; Carslaw et al., 2013). Comparatively clean and even partly pristine states can still be found over the oceans of the southern hemisphere, whereas the northern hemisphere is largely polluted (Hamilton et al., 2014; Heintzenberg et al., 2000). The strongest sources of pollution in the marine boundary layer are the plumes of large wildfires and coastal megacities as well as major shipping routes.

The formation of sea spray aerosol (SSA) through bursting bubbles at the ocean-atmosphere interface, which is driven by wind and breaking waves, is regarded as the strongest marine aerosol source in terms of mass (e.g., Monks et al., 2009). SSA comprises both organics and inorganics with a strong size dependence in composition, whereas sea salt refers to the inorganic constituents only (Bates et al., 2012; Prather et al., 2013). SSA composition depends on physicochemical and biological processes in seawater and its formation process still holds a variety of open questions (Meskhidze et al., 2013). As part of the SSA, a variety of marine microorganisms is emitted, which can be mixed with advected continental bioaerosols, resulting in a diverse and variable microbial community in the marine boundary layer (Freitas et al., 2022; Lang-Yona et al., 2022; Mayol et al., 2017).

SSA is directly emitted from the ocean to the atmosphere and thus considered a primary aerosol source. In addition, precursor gasses emitted from the ocean can undergo chemical reactions, gas-to-particle conversion, and secondary aerosol formation in the atmosphere, representing another major aerosol source (e.g., Monks et al., 2009). The most prominent example is the oxidation of dimethylsulphide (DMS) from marine emissions with a subsequent formation of sulfate aerosol (Charlson et al., 1987; McCoy et al., 2015). Furthermore, volatile organic compounds can act as precursors for secondary organic aerosol formation and the nucleation of new particles can occur in the lower, middle, and upper troposphere (O'Dowd & de Leeuw, 2007; Williamson et al., 2019; Zheng et al., 2021). The mixture of secondary particles from all these sources undergoes profound physicochemical transformations via photochemical oxidation, heterogeneous chemical reactions, and aqueous phase chemistry (Pöschl, 2005; Ramachandran, 2018; Rinaldi et al., 2011; Su et al., 2020), which enhances the complexity linking aerosol properties, sources, and effects on climate change, and vice versa.

The *S/Y ES* expeditions from 2019 to 2021 have produced a broad spectrum of atmospheric analyses including fine and coarse mode aerosol analyses. The spatial distribution of potential aerosol sources around the cruise track was identified using an adapted potential source contribution function model (Fan et al., 1995). The model was modified to account for the moving receptor on the *S/Y ES*. By combining aerosol number concentrations in fine and coarse modes with HYSPLIT back-trajectories (BTs), potential source locations for each mode were determined. The output is a BT footprint indicating regions where BTs resulted in high concentrations of fine or coarse mode aerosols at the receptor when they traversed those areas. The analyses indicate that the Greenland, Iceland, and Norwegian Seas contributed to the coarse mode aerosols, whereas the entire North Atlantic Ocean south of the polar circle served as potential source for the fine mode aerosol (Figures 13 and 14). The fine mode aerosol concentration was also high in the North Sea near the German coast relative to the other cruise track locations, indicating prominent contribution of continental emissions. Both fine mode and coarse mode aerosols had a strong source near the northwestern African continent (Figures 13 and 14). In particular, the coarse mode aerosols in the dust transported from the African continent confirm massive dust emissions to the North Atlantic Ocean.

Robust measurements of particle concentrations and size distributions across the relevant size range are of prime importance for aerosol studies. Particle number size distributions from 10 nm to ∼6 μm measured along the cruise track (Figure 2) show a consistent occurrence of three characteristic modes (Figure 14), the Aitken mode (∼10–100 nm), accumulation mode (∼100–1,000 nm), and coarse mode (>∼1,000 nm). The distinct peaks in the size distribution indicate different modes of aerosols originating from different sources and atmospheric processes (Figure 14).

The spatiotemporal distribution, community structure, and metabolic capabilities of microorganisms at the ocean-atmosphere interface were analyzed from 118 air and surface seawater filter samples from 2019 to 2021 *S/Y ES* expeditions. Cell types and abundances elucidate the microbial community diversity and composition in the air and surface seawater to reveal the potential interplay between surface water and air microbial communities. Bacterial, archeal, and eukaryotic clades are identified from their 16 and 18S ribosomal RNA marker genes. According to the

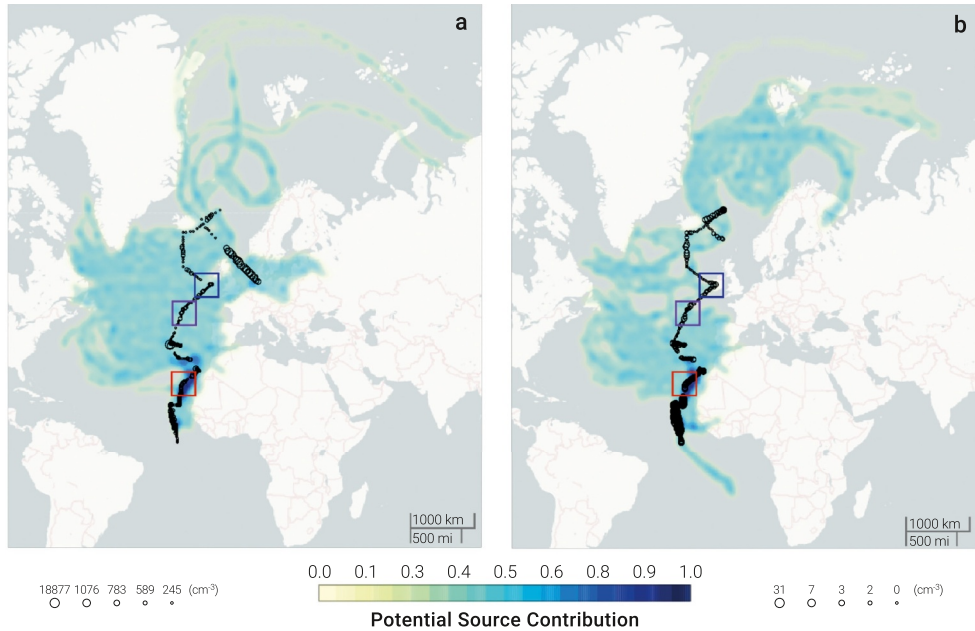

Figure 13. Source regions of air masses and aerosols along *S/Y Eugen Seibold (ES)* cruise track. (a) Particle number concentration in the fine mode (<1 μm) and (b) coarse mode (>1 μm) along cruise track (black circles) of the *S/Y ES* in 2020 and 2021. The size of the circles represents the particle number concentration levels. The potential source contribution, based on Hybrid Single-Particle Lagrangian Integrated Trajectory model (HYSPLIT, NOAA-ARL) backward trajectories (5-day intervals, 200 m start altitude, with the boat's location as the starting point) illustrates the spatiotemporal variability of regional sources for fine and coarse particles.

sequencing results, the cell abundances in the air were not directly related to those in surface seawaters suggesting that exchange of microbes between surface ocean and atmosphere was limited under the sampled conditions.

Ice nucleation assays (Kunert et al., 2018) will improve our understanding of the organisms' capability to act as IN at temperatures close to zero degrees Celsius to assess the impact of aerobiomes on the hydrological cycle (Morris et al., 2014). In combination with the data on the pico- and nano-phytoplankton (Figures 6 and 7), and data on spectrally resolved fluorescence of single bioaerosol particles (Könemann et al., 2019) from the surface ocean and overlying air will lead to a better understanding of the origin and fate of air microbial communities (Fröhlich-Nowoisky et al., 2012, 2016), as well as the environmental parameters leading to long-range transport of aerosol species. Data obtained with the *S/Y ES* are complemented by calculated backward air trajectories (Figure 13),

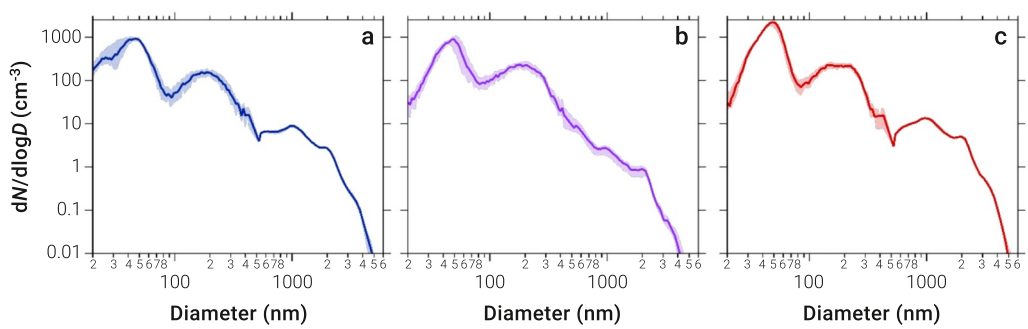

Figure 14. Particle number size distributions for three selected locations (a, b, c, from north to south) along the cruise track highlighted by squares in Figure 13 show typical trimodal marine size distributions. Each distribution comprises an Aitken mode centered at about 50 nm, an accumulation mode at about 200 nm, and a coarse mode at about 1,000 nm. The variability in the size distributions relates to differences in air mass origin and atmospheric aerosol aging.

satellite data, and information on air microbial communities from long-term measurement stations and platforms (e.g., Flores et al., 2020; Kokhanovsky, 2008; Prass et al., 2021; Souza et al., 2021).

During a dust outbreak from the Sahara Desert (*Calima*) in February 2021, filter samples were collected with the Low Volume Filter Sampler (Table 2) at the eastern side of Gran Canaria. First molecular genetic results show that the desert dust comprised a characteristic set of phyla with similarities to samples taken over the Amazon rainforest at the Amazon Tall Tower Observatory (ATTO), near Manaus, Brazil, during a dust event in February 2020. Both *Calima* and Brazilian dust events were different from samples obtained during dust free episodes in the marine Atlantic atmosphere, with notable increased relative sequence abundances of the bacterial division *Firmicutes*. Further analyses will provide insights into the microbial composition of desert dust as related to the source region soil microbiome, viability of organisms after arrival in the receptor regions, alteration during the transport across the Atlantic, and effect on the biogeochemistry of the surface ocean through the deposition.

The Sahara Desert releases about 130–1,300 Tg of dust per year, and about 8–50 Tg of it is deposited in the Amazon Basin, constituting a transatlantic transport of nutrients (Engelstaedter et al., 2006; Goudie & Middleton, 2001; Kaufman et al., 2005; Laurent et al., 2008; Prospero et al., 2020). The desert dust influences climate, as it alters the scattering and absorption of sunlight and may enhance the formation of clouds (Jia et al., 2022). The dry soils in the source region of the dust are colonized by a variety of microorganisms and biological soil crusts, which are also affected by climate (Favet et al., 2013; Rodriguez-Caballero et al., 2018, 2022).

4.6. Black Carbon in the Atmosphere

BC is the most strongly light-absorbing component of atmospheric aerosols and one of the most important short-lived climate-warming agents. Quantitative estimates of the climate impact of BC are hampered by a lack of observational data, particularly in remote areas, where observations are especially useful for constraining physical and chemical processes in models (Ditas et al., 2018). Mass concentrations and mixing state of individual BC particles were measured with an SP2 (Table 2) from March 2019 to October 2021 for over 1,900 cruise hours. The observations show that BC is widespread on the Atlantic Ocean from coastal to remote areas, with mass concentrations ranging from a few to several hundred nanograms per cubic meter (ng m^{-3}). For example, outflow of continental BC from mainland Europe and the British Isles caused high BC concentrations (34 ± 95 ng m^{-3}) over the North Sea, and lower concentrations (4 ± 5 ng m^{-3}) in the northern North Atlantic (Figure 15).

5. Conclusions and Perspectives of the *S/Y Eugen Seibold* Project

The *S/Y ES* project is designed to measure and sample properties of air, water, and plankton to further develop traditional and novel proxies, including isotopes, and trace metals, to improve our understanding of biogeochemical cycles of the atmosphere and oceans, investigate the mechanisms of biological uptake, export, and recycling of elements in the open marine water column, and to inventory non-biogenic matter sources and sinks in the oceans.

Repeated seasonal and interannual probing of the water column with the *S/Y ES*, and comparison to historical data obtained over the past decades (e.g., de Garidel-Thoron et al., 2022; Schiebel, 2002; Schiebel & Hemleben, 2000) captures the time interval of accelerated atmospheric and marine CO_2 increase and climate warming since the 1970s (e.g., Cheng et al., 2019; IPCC, 2021). Resulting changes of the atmospheric and marine conditions such as Arctic amplification and changes in the jet streams, changing stratification of the surface water column, decreasing oxygenation of the water column, declining marine food production, and ocean acidification are already being detected (Chown, 2020; Free et al., 2022; Gruber et al., 2021; Löscher et al., 2016; Moon et al., 2022; J. K. Moore et al., 2018; Resplandy, 2018; Schmidtko et al., 2017; Shi et al., 2022; Stramma et al., 2008; Zanna et al., 2019).

The first campaign of the *S/Y ES* in the eastern North Atlantic, from subpolar to tropical waters, between Iceland and the equator has produced a wealth of biogeochemical data and samples from the atmosphere and surface ocean. Data and samples obtained from 2019 to 2021 provide a systematic synoptic understanding of physical, chemical, and biological variables of the ocean climate as a major driver of global climate change. The entire suite of measurements facilitated by the technological infrastructure of the *S/Y ES* provide refined proxy calibration of planktic paleo-archives at high temporal and spatial resolution in relation to seawater and atmospheric parameters.

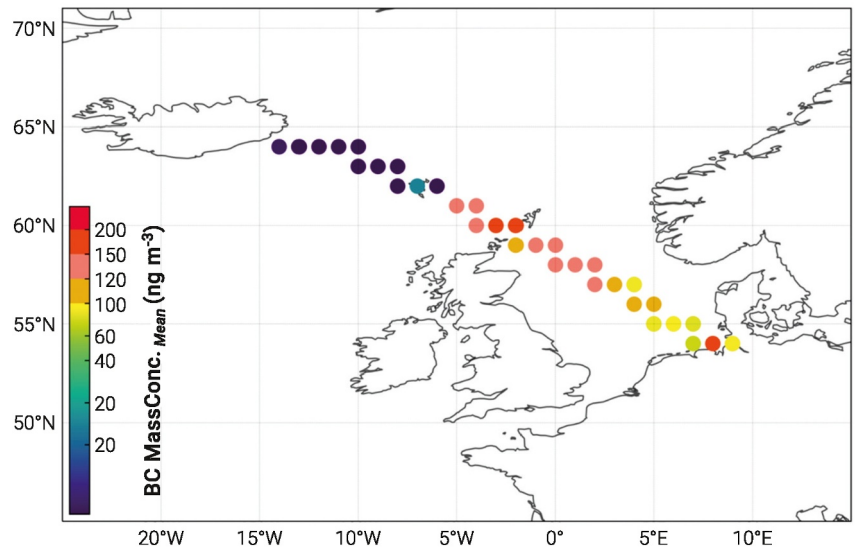

Figure 15. Black carbon (BC) data from the North Sea and North Atlantic Ocean. Spatial distribution of BC mass concentration measured with the Soot Photometer instrument (Table 2) onboard the *S/Y Eugen Seibold* in February, June, and July 2020 from the European continent to Iceland. The data are averaged and shown on a 1° by 1° grid resolution.

Data on phytoplankton photophysiology acquired by FRR fluorometry (*FRRf*) and flow cytometry show that the technological set-up on the *S/Y ES* facilitates detailed assessment of how phytoplankton optical groups are affected by environmental conditions on multiple spatial and temporal scales (Aardema et al., 2024). Differential effects of the various ecological parameters explain the interplay between photophysiology of the phytoplankton community and its environment for a detailed assessment of the processes involved in marine photosynthesis. Temporal variation is apparent in multiple photophysiological processes at sub-daily to daily time-periods, and the strength of this diel cycle differs between biogeographical provinces (Figure 2). Differences in photo-acclimation strategies between regions are being identified. The implications for primary productivity and thereby ecosystem functioning and biogeochemical cycling are being discussed with particular emphasis on the photo-acclimation response (e.g., carbon-to-chlorophyll ratio), which appears to account for a significant percentage of the observed (e.g., interannual) chlorophyll anomalies observed by remote sensing (Behrenfeld et al., 2016; Britten et al., 2022).

Phytoplankton abundances at nano size (≤20 μm) and below, are enumerated using semi-continuous flow cytometry. Vertical profiles of the photic layer comprise different biomes along the *20-West-Transect* and reveal differences between subpolar to tropical biomes and seasons, for example, strong alternation between cyano-bacterial and nano-eukaryotic prevalence (Figure 6). Total phytoplankton abundances in the surface mixed layer ranged from $<10 \times 10^3$ cells mL^{-1} in the oligotrophic subtropical gyre, and up to 150×10^3 cells mL^{-1} in the northern North Atlantic in spring, the Mauritanian upwelling, as well as at the DCM, the latter being dominated by cyanobacteria such as *Prochlorococcus* in the more oligotrophic biomes.

The combination of high spatial and temporal resolution sampling of phytoplankton communities and dissolved gases, together with a large suite of environmental data, facilitates a comprehensive evaluation of how changes in biological activity influence the variability of active gases (e.g., CO_2 and O_2) in the surface ocean. The concomitant underway determination of sea surface dissolved argon and oxygen, acquired with the flow equil-ibrator membrane inlet *miniRUEDI* mass spectrometer (Table 2), allows for high resolution computation of microbial net community production (NCP), which is the metabolic balance of the plankton community resulting from both autotrophic carbon fixation through photosynthesis and carbon loss through respiration. NCP captures the health and metabolic state of the plankton community as a whole, and does not always equate to chl-*a* levels or phytoplankton abundance (Poulton et al., 2006), but represents the net rate of biological organic carbon pro-duction potentially available for export to the deep ocean (Emerson, 2014). The direct influence of NCP on air-sea CO_2 fluxes both in parallel at high spatial and temporal resolution is assessed along the sampled transect. Results suggest that the effect of upwelled waters in tropical latitudes triggers a phytoplanktonic community that is able to

fix as much carbon as the community in high latitude waters. Understanding of these processes is of pivotal importance in order to evaluate the ocean's capacity in sequestering atmospheric CO_2 and the potential for carbon export to the deep sea.

5.1. Data on Trace Elements and Stable Isotopes

Bioactive trace elements, such as micronutrients, are critical for marine life and affect the functioning of ocean ecosystems and the global carbon cycle. Some trace elements are also of concern as contaminants, while others, together with a diverse array of isotopes, are used to assess modern-ocean processes and the role of the ocean in past climate change. Despite the recognized importance of trace elements and isotopes in the ocean, our ability to employ them is limited by uncertainty about their sources, sinks, internal cycling, and chemical speciation.

In addition to macronutrients (NO_3, PO_4, and C), trace metals such as iron (Fe), cadmium (Cd), molybdenum (Mo), nickel (Ni), chromium (Cr), cobalt (Co), manganese (Mn), and zinc (Zn) are essential elements for primary production (de Baar et al., 2017; Sunda, 2012; Twining & Baines, 2013). The micronutrients regulate metabolic pathways and are part of vital enzymes involved in key biological processes such as photosynthetic carbon sequestration (Fe, Zn, Cd), nitrogen fixation (Fe, Mo), methanogenesis (Ni), and oxygen regulation in photosynthesis and general metabolic processes (Mn). However, in seawater, micronutrients are present at low concentrations and their bioavailability can limit marine phytoplankton growth. This is of particular significance for oceanic High-Nutrient-Low-Chlorophyll (HNLC) regions such as the eastern equatorial Pacific and Southern Ocean, where iron—as an essential micronutrient supplied to the oceans mostly via atmospheric dusts—is insufficient, and, paradoxically, results in low primary production and biomass in these macronutrient rich regions (Martin & Fitzwater, 1988; Martínez-García et al., 2009, 2014). Natural mass-dependent stable isotope variations of trace metal micronutrients are analyzed to provide novel tracers of biological uptake and utilization, and application in paleoclimate reconstruction.

5.2. Ocean Heat and Temperature Proxies

Ocean heat transport processes are paramount in Earth's climate as they distribute energy around the globe. As the upper 30 m of the oceans contain as much heat as the entire atmosphere, the temperature of the upper ocean is among the most decisive variables in the Earth's climate system, by regulating ocean-atmosphere heat exchange, development of pressure gradients and wind fields, as well as formation and circulation of water masses that comprise the oceanic thermohaline circulation (THC; Broecker, 1991; von Schuckmann et al., 2020). As temperature affects both surface and deep oceanic circulation, as well as heat and moisture transport around the globe, and the state of global climate as a whole, SST fluctuations are critical to understand how heat is distributed. Therefore, temperature reconstruction in marine paleoclimatology is key to assess the variability of heat transport processes through time. Consequently, validation and calibration of inorganic and organic geochemical temperature proxies with modern observations and environmental data is of high priority in climate reconstruction. Precision in past SST reconstruction is also vital to improve the accuracy of numerical simulations of past climate and the effect on human societies through general circulation models (GCMs; Timmermann et al., 2022), to address the extent and impact of anthropogenically forced climate change. In addition, stringent testing by close comparison to quantitative SST reconstruction via proxy data fosters systematic understanding of climate evolution, which critically depends on the accuracy and reliability of such proxies. The *S/Y ES* campaigns provide samples and data for the next level of in situ proxy calibration.

5.3. Alkenone and TEX_{86} SST Calibration

The alkenone unsaturation index $U^{k'}_{37}$ has been widely adopted by paleoceanographers as a proxy to estimate past SSTs. Since it was first demonstrated that alkenone ratios in sediments changed in a systematic way with inferred temperature, efforts have been undertaken to confirm and calibrate the $U^{k'}_{37}$ index. The temperature dependent nature of the relative abundance of the C37:2 and C37:3 alkenones has been shown by culture studies, and analyses of surface sediment and particulate organic matter sampled from the water column (Brassell et al., 1986; Müller et al., 1997; Prahl & Wakeham, 1987). Despite such positive results, the application of alkenone indices is not devoid of uncertainties. A number of recent studies highlight some degree of nonlinearity in the relationship of alkenones to SST at high (>25°C) and low (<8°C) temperature extremes, and a strong seasonal bias in the SST recorded by the $U^{k'}_{37}$ in certain oceanographic settings (Conte et al., 2006; Richey & Tierney, 2016; Rosell-Melé

& Prahl, 2013). Therefore, systematic calibration of the alkenone paleothermometer in comparison to the entire suite of environmental data obtained within the *S/Y ES* may improve our interpretation of past changes in SST.

The TEX_{86} SST index and related proxies offer a promising tool for paleoceanographic reconstructions (Schouten et al., 2002, 2013). A potential caveat to this method is that archaea producing glycerol dialkyl glycerol tetraether lipids (GDGTs) are ubiquitous and, in contrast to the photosynthetic alkenone producers, live in the entire water column, and not only in the euphotic surface layer (Karner et al., 2001). Surveys of particulate organic matter in the ocean as well as recent global core-top calibrations of TEX_{86} suggest that the temperature of the surface mixed layer (the upper 120 m) is generally integrated in the sedimentary GDGT signal (Kim et al., 2010; Wuchter et al., 2005; Zonneveld et al., 2010). However, it has been found that not all regions follow the same pattern, and data sets evaluating the potential effect of seasonality are scarce (e.g., Hernández-Sánchez et al., 2014; Huguet et al., 2007; Taylor et al., 2013). Therefore, we will constrain the water depths and seasonality of GDGT production in different ocean regions, and its relationship to the signal recorded in the sediment.

5.4. Dust Biomarkers

Dust plays an important role in global climate by influencing the radiative balance of the atmosphere. It also serves as an important source of limiting micronutrients (e.g., iron) in the open ocean (e.g., Martin & Fitzwater, 1988; M. Moore et al., 2009; Pabortsava et al., 2017), and drives marine productivity, for example, in the HNLC regions such as the Southern Ocean and the equatorial and North Pacific.

The flux, distribution, and isotopic composition of certain wind-borne terrigenous biomarkers (e.g., long-chain *n*-alkanes, *n*-alkanols, and *n*-alkanoic acids) can provide information on the input of continental matter to the ocean, and changes in the environmental conditions at the source region of the dust (Abouchami et al., 2013; Yu et al., 2020). For example, the carbon isotopic composition of these compounds is affected by ambient atmospheric $^{13/12}CO_2$, the pathway during photosynthesis (C3 or C4 biosynthetic pathway), and factors (including aridity) that affect the conductance of the plant's stomata used to reconstruct changes in vegetation types (Schwab et al., 2015). In addition, the δD values of the plant lipids are affected by the environmental water, and further modulated by local hydrological processes and isotope effects associated with biosynthesis. Therefore, δD values can be used in marine and lake records to reconstruct changes in the hydrological cycle (Schwab et al., 2015). Understanding the distribution and isotopic composition of these terrestrial biomarkers in modern dust samples from different ocean regions and marine proxies will significantly improve the accuracy of paleoclimate reconstructions.

5.5. Recent Developments and Upcoming Projects

The *S/Y ES* has crossed the Atlantic and Caribbean Sea over Christmas and New Year 2022/2023, and sampled a profile along 13°N, for a better understanding of the effect of Saharan dust on the marine nutrient budget and the ^{15}N signal as a proxy of past productivity changes of the tropical Atlantic, and modern climate related effects such as the *Sargassum* bloom. In March 2023, the *S/Y ES* has arrived in the tropical Eastern Pacific (TEP) with the aim to describe the biogeochemistry (e.g., nutrients, ^{15}N, and oxygen minimum zones) of an entire El Niño cycle and the El Niño-Southern Oscillation (ÈNSO). The campaign in the TEP is conveyed in close cooperation with the Smithsonian Tropical Research Institute, based on a Memorandum of Understanding (2021) and Cooperation Agreement (2023), and supported by the Darwin Center at Galapagos.

Conflict of Interest

The authors declare no conflicts of interest relevant to this study.

Data Availability Statement

No custom code has been used. All data presented in this paper have been published in the Edmond Open Research Data Repository of the Max Planck Society (https://doi.org/10.17617/3.30MFES). A growing collection of the whole data of existing and future ES cruises will be published as relational datasets in the open access repository PANGAEA (www.pangaea.de). An overview of the campaigns is provided by the link https://www.pangaea.de/expeditions/bybasis/Eugen%20Seibold.

Acknowledgments
Captains Kaarel Kruusmägi, Mihkel Pajula, and Karl Vahtra, and crew Argo Kruusmägi, Margus Zahharov, Janette Possul, Marge Piirmets, Adeele Kuslap, Marharyta Kalashnikova have substantially contributed to the success of the 2019, 2020, and 2021 sampling campaigns. Frank Helleis, Florian Rubach, Florian Ditas, Jan-David Förster, Sergej Molleker, Michael Welling, Bastian Meckel, Dirk Schoch, and Ralf Wittkowski have been providing technological support of the project at the MPIC and onboard. We are grateful to Stefan Marx and colleagues at SubCtech (Kiel, Germany), and George Dubelaar and colleagues at CytoBuoy (Woerden, The Netherlands) for their generous intellectual and technological support. Sonja Endres supported the project during an early construction stage of the boat. Anna Friedrichs contributed to setting up the database and data analysis scripts. Carlos Barrera (PLOCAN, Gran Canaria) provided indispensable technical support. Mar Benavides (IRD, MIO, Marseille), Mehmet Köse (MPIC), Holger Anlauf (KAUST), Louis Flament (ENS, Lyon), and Sylvain Pichat (ENS, Lyon and MPIC) provided intellectual input and hands-on help with the analyses of various plankton types. Leon Prädel and Gabriele Herrmann (both MPIP, Mainz) provided analyses to set up contamination-free inline water sampling. Susanne Benner, Dominik Jack, and Anette Spiess (all MPIC) have been coordinating public outreach and design of the project. We are grateful to Cordula Zenk (GEOMAR) for her invaluable help with the logistics at Mindelo and research permissions in the EEZ of Cabo Verde. Administrative support has gratefully been provided by Jens Egler, Ira Lemm, Sonja Jung, Gisela Böhmer, Harald Eymert, Anett Bersch, Marietta Winkler, and Anette Beck at MPIC. Thomas Liebe and colleagues at F. Laeisz shipping are gratefully acknowledged for their unremitting support of operations. Gauvain Wiemer, Maximilian Betz, Gisbert Breitbach, Stefanie Schumacher, Daniela Ransby, Hela Mertens, Amelie Driemel, Janine Felden, and Frank Oliver Glöckner have been of great support with data management within the German research project *DAM-Underway-Research Data*, funded by the German Federal Ministry of Education and Research (BMBF, 2021–2022, 03F0880F to Ralf Schiebel), and the *PANGAEA* World Data Center. Christian Begler from GEOMAR supported sampling by providing information SLA data on the position of eddies via the BELUGA platform. BELUGA Navigator has been developed in the underwater robotics group at GEOMAR. Michael Schmidt, Lorenzo Argento, Annette Axthelm, and Henner Rolvien built the boat in communication with Frank Helleis, Ralf Schiebel, and Gerald Haug. Construction and maintenance of the

References

Aardema, H. M., Slagter, H. A., Hrabe de Angelis, I., Calleja, M. Ll., Dragoneas, A., Moretti, S., et al. (2024). On the variability of phytoplankton photophysiology along a latitudinal transect in the North Atlantic surface ocean. *Journal of Geophysical Research: Biogeosciences*, *129*, e2023JG007962. https://doi.org/10.1029/2023JG007962

Abouchami, W., Näthe, K., Kumar, A., Galer, S. J. G., Jochum, K. P., Williams, E., et al. (2013). Geochemical and isotopic characterization of the Bodélé Depression dust source and implications for transatlantic dust transport to the Amazon Basin. *Earth and Planetary Science Letters*, *380*, 112–123. https://doi.org/10.1016/j.epsl.2013.08.028

Altabet, M. A., & Francois, R. (1994). Sedimentary nitrogen isotopic ratio as a recorder for surface ocean nitrate utilization. *Global Biogeochemical Cycles*, *8*(1), 103–116. https://doi.org/10.1029/93GB03396

Altabet, M. A., Murray, D. W., & Prell, W. L. (1999). Climatically linked oscillations in Arabian Sea denitrification over the past 1 m.y.: Implications for the marine N cycle. *Paleoceanography*, *14*(6), 732–743. https://doi.org/10.1029/1999PA900035

Anand, P., Elderfield, H., & Conte, M. H. (2003). Calibration of Mg/Ca thermometry in planktonic foraminifera from a sediment trap time series: Calibration of Mg/Ca thermometry in planktonic foraminifera. *Paleoceanography*, *18*(2), 1050. https://doi.org/10.1029/2002PA000846

Andreae, M. O. (2007). Aerosols before pollution. *Science*, *315*(5808), 50–51. https://doi.org/10.1126/science.1136529

Auderset, A., Moretti, S., Taphorn, B., Ebner, P.-R., Kast, E., Wang, X. T., et al. (2022). Enhanced ocean oxygenation during Cenozoic warm periods. *Nature*, *609*(7925), 77–82. https://doi.org/10.1038/s41586-022-05017-0

Bates, T. S., Quinn, P. K., Frossard, A. A., Russell, L. M., Hakala, J., Petäjä, T., et al. (2012). Measurements of ocean derived aerosol off the coast of California: Measurements of ocean derived aerosol. *Journal of Geophysical Research*, *117*(D21), 13. https://doi.org/10.1029/2012JD017588

Behrenfeld, M. J., O'Malley, R. T., Boss, E. S., Westberry, T. K., Graff, J. R., Halsey, K. H., et al. (2016). Revaluating ocean warming impacts on global phytoplankton. *Nature Climate Change*, *6*(3), 323–330. https://doi.org/10.1038/nclimate2838

Behrenfeld, M. J., O'Malley, R. T., Siegel, D. A., McClain, C. R., Sarmiento, J. L., Feldman, G. C., et al. (2006). Climate-driven trends in contemporary ocean productivity. *Nature*, *444*(7120), 752–755. https://doi.org/10.1038/nature05317

Biard, T., Stemmann, L., Picheral, M., Mayot, N., Vandromme, P., Hauss, H., et al. (2016). In situ imaging reveals the biomass of giant protists in the global ocean. *Nature*, *532*(7600), 504–507. https://doi.org/10.1038/nature17652

Bieler, A. L. (2022). *Tissue-bound nitrogen isotopic signals of planktic foraminifers and pteropods in the subtropical eastern North Atlantic (MSc thesis)*. ETH Zürich and MPIC Mainz.

Bolton, A., Baker, J. A., Dunbar, G. B., Carter, L., Smith, E. G. C., & Neil, H. L. (2011). Environmental versus biological controls on Mg/Ca variability in *Globigerinoides ruber* (white) from core top and plankton tow samples in the southwest Pacific Ocean: Variability of Mg/Ca in *Gs. ruber*. *Paleoceanography*, *26*(2), 89–102. https://doi.org/10.1029/2010PA001924

Brassell, S. C., Eglinton, G., Marlowe, I. T., Pflaumann, U., & Sarnthein, M. (1986). Molecular stratigraphy: A new tool for climatic assessment. *Nature*, *320*(6058), 129–133. https://doi.org/10.1038/320129a0

Brennwald, M. S., Schmidt, M., Oser, J., & Kipfer, R. (2016). A portable and autonomous mass spectrometric system for on-site environmental gas analysis. *Environmental Science & Technology*, *50*(24), 13455–13463. https://doi.org/10.1021/acs.est.6b03669

Britten, G. L., Padalino, C., Forget, G., & Follows, M. J. (2022). Seasonal photoacclimation in the North Pacific transition zone. *Global Biogeochemical Cycles*, *36*(6), e2022GB007324. https://doi.org/10.1029/2022GB007324

Broecker, W. (1991). The great ocean conveyor. *Oceanography*, *4*(2), 79–89. https://doi.org/10.5670/oceanog.1991.07

Brooks, S. D., & Thornton, D. C. O. (2018). Marine aerosols and clouds. *Annual Review of Marine Science*, *10*(1), 289–313. https://doi.org/10.1146/annurev-marine-121916-063148

Brun, P., Stamieszkin, K., Visser, A. W., Licandro, P., Payne, M. R., & Kiørboe, T. (2019). Climate change has altered zooplankton-fuelled carbon export in the North Atlantic. *Nature Ecology & Evolution*, *3*(3), 416–423. https://doi.org/10.1038/s41559-018-0780-3

Buitenhuis, E. T., Li, W. K. W., Vaulot, D., Lomas, M. W., Landry, M. R., Partensky, F., et al. (2012). Picophytoplankton biomass distribution in the global ocean. *Earth System Science Data*, *4*(1), 37–46. https://doi.org/10.5194/essd-4-37-2012

Busch, K. W., & Busch, M. A. (1999). Cavity-ringdown spectroscopy. *American Chemical Society*. Retrieved from https://pubs.acs.org/isbn/9780841236004

Carslaw, K. S., Lee, L. A., Reddington, C. L., Pringle, K. J., Rap, A., Forster, P. M., et al. (2013). Large contribution of natural aerosols to uncertainty in indirect forcing. *Nature*, *503*(7474), 67–71. https://doi.org/10.1038/nature12674

Charlson, R. J., Lovelock, J. E., Andreae, M. O., & Warren, S. G. (1987). Oceanic phytoplankton, atmospheric sulphur, cloud albedo and climate. *Nature*, *326*(6114), 655–661. https://doi.org/10.1038/326655a0

Cheng, L., Abraham, J., Hausfather, Z., & Trenberth, K. E. (2019). How fast are the oceans warming? *Science*, *363*(6423), 128–129. https://doi.org/10.1126/science.aav7619

Chown, S. L. (2020). Marine food webs destabilized. *Science*, *369*(6505), 770–771. https://doi.org/10.1126/science.abd5739

CLIMAP Project. (1981). *Seasonal reconstructions of the Earth's surface at the last glacial maximum*. Geological Society of America.

Conte, M. H., Sicre, M.-A., Rühlemann, C., Weber, J. C., Schulte, S., Schulz-Bull, D., & Blanz, T. (2006). Global temperature calibration of the alkenone unsaturation index ($U^{K'}_{37}$) in surface waters and comparison with surface sediments: Alkenone unsaturation index. *Geochemistry, Geophysics, Geosystems*, *7*(2), Q02005. https://doi.org/10.1029/2005GC001054

de Baar, H. J. W., van Heuven, S. M. A. C., & Middag, R. (2017). Ocean biochemical cycling and trace elements. In P. Bobrowsky & B. Marker (Eds.), *Encyclopedia of engineering geology* (pp. 1–21). Springer International Publishing. https://doi.org/10.1007/978-3-319-39193-9_356-1

de Garidel-Thoron, T., Chaabane, S., Giraud, X., Meilland, J., Jonkers, L., Kucera, M., et al. (2022). The foraminiferal response to climate stressors project: Tracking the community response of planktonic foraminifera to historical climate change. *Frontiers in Marine Science*, *9*, 827962. https://doi.org/10.3389/fmars.2022.827962

Deutsch, C., Sigman, D. M., Thunell, R. C., Meckler, A. N., & Haug, G. H. (2004). Isotopic constraints on glacial/interglacial changes in the oceanic nitrogen budget: Glacial/Interglacial nitrogen budget. *Global Biogeochemical Cycles*, *18*(4), GB4012. https://doi.org/10.1029/2003GB002189

de Vargas, C., Audic, S., Henry, N., Decelle, J., Mahé, F., Logares, R., et al. (2015). Eukaryotic plankton diversity in the sunlit ocean. *Science*, *348*(6237), 1261605. https://doi.org/10.1126/science.1261605

Ditas, J., Ma, N., Zhang, Y., Assmann, D., Neumaier, M., Riede, H., et al. (2018). Strong impact of wildfires on the abundance and aging of black carbon in the lowermost stratosphere. *Proceedings of the National Academy of Sciences*, *115*(59), E11595–E11603. https://doi.org/10.1073/pnas.1806868115

Dybwad, M., Skogan, G., & Blatny, J. M. (2014). Comparative testing and evaluation of nine different air samplers: End-to-End sampling efficiencies as specific performance measurements for bioaerosol applications. *Aerosol Science and Technology*, *48*(3), 282–295. https://doi.org/10.1080/02786826.2013.871501

S/Y Eugen Seibold has been generously funded by the Werner Siemens-Stiftung (WSS, Zug, Switzerland). Financial support of the *S/Y Eugen Seibold* operations is provided by the Max Planck Society for the Advancement of Science (MPG, Munich, Germany).

Elderfield, H., Vautravers, M., & Cooper, M. (2002). The relationship between shell size and Mg/Ca, Sr/Ca, δ ^{18} O, and δ ^{13} C of species of planktonic foraminifera: Planktonic foraminifera. *Geochemistry, Geophysics, Geosystems*, *3*(8), 1–13. https://doi.org/10.1029/2001GC000194

Emerson, S. (2014). Annual net community production and the biological carbon flux in the ocean. *Global Biogeochemical Cycles*, *28*(1), 14–28. https://doi.org/10.1002/2013GB004680

Engelstaedter, S., Tegen, I., & Washington, R. (2006). North African dust emissions and transport. *Earth-Science Reviews*, *79*(1), 73–100. https://doi.org/10.1016/j.earscirev.2006.06.004

Fan, A., Hopke, P. K., Raunemaa, T. M., Öblad, M., & Pacyna, J. M. (1995). A study on the potential sources of air pollutants observed at Tjörn, Sweden. *Environmental Science and Pollution Research*, *2*(2), 107–115. https://doi.org/10.1007/BF02986733

Favet, J., Lapanje, A., Giongo, A., Kennedy, S., Aung, Y.-Y., Cattaneo, A., et al. (2013). Microbial hitchhikers on intercontinental dust: Catching a lift in Chad. *The ISME Journal*, *7*(4), 850–867. https://doi.org/10.1038/ismej.2012.152

Felden, J., Möller, L., Schindler, U., Huber, R., Schumacher, S., Koppe, R., et al. (2023). PANGAEA—Data publisher for Earth & environmental science. *Scientific Data*, *10*(1), 347. https://doi.org/10.1038/s41597-023-02269-x

Field, C. B., Behrenfeld, M. J., Randerson, J. T., & Falkowski, P. (1998). Primary production of the biosphere: Integrating terrestrial and oceanic components. *Science*, *281*(5374), 237–240. https://doi.org/10.1126/science.281.5374.237

Fischer, A., Schiebel, R., Jochum, K. P., Heins, L., Arns, A. I., Aardema, H. M., et al. (2024). Single chamber Mg/Ca analyses of *Globigerinoides ruber* for paleo-proxy calibration using femtosecond La-ICP-MS. *Scientific Data*, *11*(583), 583. https://doi.org/10.1038/s41597-024-03402-0

Fischer, G. & Wefer, G. (Eds.) (1999). *Use of proxies in paleoceanography*. Springer. https://doi.org/10.1007/978-3-642-58646-0

Flores, J. M., Bourdin, G., Altaratz, O., Trainic, M., Lang-Yona, N., Dzimban, E., et al. (2020). Tara Pacific expedition's atmospheric measurements of marine aerosols across the atlantic and Pacific oceans: Overview and preliminary results. *Bulletin of the American Meteorological Society*, *101*(5), E536–E554. https://doi.org/10.1175/BAMS-D-18-0224.1

Franco, M. A., Ditas, F., Kremper, L. A., Machado, L. A. T., Andreae, M. O., Araújo, A., et al. (2022). Occurrence and growth of sub-50 nm aerosol particles in the Amazonian boundary layer. *Atmospheric Chemistry and Physics*, *22*(5), 3469–3492. https://doi.org/10.5194/acp-22-3469-2022

Free, C. M., Cabral, R. B., Froehlich, H. E., Battista, W., Ojea, E., O'Reilly, E., et al. (2022). Expanding ocean food production under climate change. *Nature*, *605*(7910), 490–496. https://doi.org/10.1038/s41586-022-04674-5

Freitas, G. P., Stolle, C., Kaye, P. H., Stanley, W., Herlemann, D. P. R., Salter, M. E., & Zieger, P. (2022). Emission of primary bioaerosol particles from Baltic seawater. *Environmental Science: Atmospheres*, *2*(5), 1170–1182. https://doi.org/10.1039/D2EA00047D

Frémont, P., Gehlen, M., Vrac, M., Leconte, J., Delmont, T. O., Wincker, P., et al. (2022). Restructuring of plankton genomic biogeography in the surface ocean under climate change. *Nature Climate Change*, *12*(4), 393–401. https://doi.org/10.1038/s41558-022-01314-8

Friedrich, O., Schiebel, R., Wilson, P. A., Weldeab, S., Beer, C. J., Cooper, M. J., & Fiebig, J. (2012). Influence of test size, water depth, and ecology on Mg/Ca, Sr/Ca, δ^{18}O and δ^{13}C in nine modern species of planktic foraminifers. *Earth and Planetary Science Letters*, *319–320*, 133–145. https://doi.org/10.1016/j.epsl.2011.12.002

Fripiat, F., Martínez-García, A., Marconi, D., Fawcett, S. E., Kopf, S. H., Luu, V. H., et al. (2021). Nitrogen isotopic constraints on nutrient transport to the upper ocean. *Nature Geoscience*, *14*(11), 855–861. https://doi.org/10.1038/s41561-021-00836-8

Fröhlich-Nowoisky, J., Burrows, S. M., Xie, Z., Engling, G., Solomon, P. A., Fraser, M. P., et al. (2012). Biogeography in the air: Fungal diversity over land and oceans. *Biogeosciences*, *9*(3), 1125–1136. https://doi.org/10.5194/bg-9-1125-2012

Fröhlich-Nowoisky, J., Kampf, C. J., Weber, B., Huffman, J. A., Pöhlker, C., Andreae, M. O., et al. (2016). Bioaerosols in the Earth system: Climate, health, and ecosystem interactions. *Atmospheric Research*, *182*, 346–376. https://doi.org/10.1016/j.atmosres.2016.07.018

Gorbunov, M. Y., & Falkowski, P. G. (2022). Using chlorophyll fluorescence to determine the fate of photons absorbed by phytoplankton in the World's Oceans. *Annual Review of Marine Science*, *14*(1), 213–238. https://doi.org/10.1146/annurev-marine-032621-122346

Goudie, A. S., & Middleton, N. J. (2001). Saharan dust storms: Nature and consequences. *Earth-Science Reviews*, *56*(1–4), 179–204. https://doi.org/10.1016/s0012-8252(01)00067-8

Gray, W. R., Weldeab, S., Lea, D. W., Rosenthal, Y., Gruber, N., Donner, B., & Fischer, G. (2018). The effects of temperature, salinity, and the carbonate system on Mg/Ca in Globigerinoides ruber (white): A global sediment trap calibration. *Earth and Planetary Science Letters*, *482*, 607–620. https://doi.org/10.1016/j.epsl.2017.11.026

Gross, L. (2007). Untapped bounty: Sampling the seas to survey microbial biodiversity. *PLoS Biology*, *5*(3), e85. https://doi.org/10.1371/journal.pbio.0050085

Gruber, N., Boyd, P. W., Frölicher, T. L., & Vogt, M. (2021). Biogeochemical extremes and compound events in the ocean. *Nature*, *600*(7889), 395–407. https://doi.org/10.1038/s41586-021-03981-7

Guidi, L., Chaffron, S., Bittner, L., Eveillard, D., Larhlimi, A., Roux, S., et al. (2016). Plankton networks driving carbon export in the oligotrophic ocean. *Nature*, *532*(7600), 465–470. https://doi.org/10.1038/nature16942

Hamilton, D. S., Lee, L. A., Pringle, K. J., Reddington, C. L., Spracklen, D. V., & Carslaw, K. S. (2014). Occurrence of pristine aerosol environments on a polluted planet. *Proceedings of the National Academy of Sciences*, *111*(52), 18466–18471. https://doi.org/10.1073/pnas.1415440111

Hamilton, D. S., Perron, M. M. G., Bond, T. C., Bowie, A. R., Buchholz, R. R., Guieu, C., et al. (2022). Earth, wind, fire, and pollution: Aerosol nutrient sources and impacts on ocean biogeochemistry. *Annual Review of Marine Science*, *14*(1), 303–330. https://doi.org/10.1146/annurev-marine-031921-013612

Heintzenberg, J., Covert, D. C., & Van Dingenen, R. (2000). Size distribution and chemical composition of marine aerosols: A compilation and review. *Tellus B: Chemical and Physical Meteorology*, *52*(4), 1104. https://doi.org/10.3402/tellusb.v52i4.17090

Hernández-Sánchez, M. T., Woodward, E. M. S., Taylor, K. W. R., Henderson, G. M., & Pancost, R. D. (2014). Variations in GDGT distributions through the water column in the south east Atlantic Ocean. *Geochimica et Cosmochimica Acta*, *132*, 337–348. https://doi.org/10.1016/j.gca.2014.02.009

Huguet, C., Schimmelmann, A., Thunell, R., Lourens, L. J., Sinninghe Damsté, J. S., & Schouten, S. (2007). A study of the TEX_{86} paleothermometer in the water column and sediments of the Santa Barbara basin, California: A high-resolution record. *Paleoceanography*, *22*(3), PA3203. https://doi.org/10.1029/2006PA001310

Huisman, J., Pham Thi, N. N., Karl, D. M., & Sommeijer, B. (2006). Reduced mixing generates oscillations and chaos in the oceanic deep chlorophyll maximum. *Nature*, *439*(7074), 322–325. https://doi.org/10.1038/nature04245

IPCC. (2021). Climate change 2021: The physical science basis. In *Contribution of working group I to the sixth assessment report of the intergovernmental panel on climate change*. Cambridge University Press. Retrieved from. https://doi.org/10.1017/9781009157896

Jia, G., Shevliakova, E., Artaxo, P., De Noblet-Ducoudré, N., Houghton, R., House, J., et al. (2022). Land–climate interactions. In *Climate change and land: IPCC special report on climate change, desertification, land degradation, sustainable land management, food security, and greenhouse gas fluxes in terrestrial ecosystems* (pp. 131–248). Cambridge University Press. https://doi.org/10.1017/9781009157988.004

Jochum, K. P., Jentzen, A., Schiebel, R., Stoll, B., Weis, U., Leitner, J., et al. (2019). High-resolution Mg/Ca measurements of foraminifer shells using femtosecond LA-ICP-MS for paleoclimate proxy development. *Geochemistry, Geophysics, Geosystems*, *20*(4), 2053–2063. https://doi.org/10.1029/2018GC008091

Karner, M. B., DeLong, E. F., & Karl, D. M. (2001). Archaeal dominance in the mesopelagic zone of the Pacific Ocean. *Nature*, *409*(6819), 507–510. https://doi.org/10.1038/35054051

Kaufman, Y. J., Koren, I., Remer, L. A., Tanré, D., Ginoux, P., & Fan, S. (2005). Dust transport and deposition observed from the terra-moderate resolution imaging Spectroradiometer (MODIS) spacecraft over the Atlantic Ocean. *Journal of Geophysical Research*, *110*(D10), 10–12. https://doi.org/10.1029/2003JD004436

Kim, J.-H., van der Meer, J., Schouten, S., Helmke, P., Willmott, V., Sangiorgi, F., et al. (2010). New indices and calibrations derived from the distribution of crenarchaeal isoprenoid tetraether lipids: Implications for past sea surface temperature reconstructions. *Geochimica et Cosmochimica Acta*, *74*(16), 4639–4654. https://doi.org/10.1016/j.gca.2010.05.027

Knutson, E. O., & Whitby, K. T. (1975). Aerosol classification by electric mobility: Apparatus, theory, and applications. *Journal of Aerosol Science*, *6*(6), 443–451. https://doi.org/10.1016/0021-8502(75)90060-9

Koeve, W., & Ducklow, H. W. (2001). JGOFS synthesis and modeling: The North Atlantic ocean. *JGOFS Research in the North Atlantic Ocean: A Decade of Research, Synthesis and Modelling*, *48*(10), 2141–2154. https://doi.org/10.1016/S0967-0645(00)00186-7

Kokhanovsky, A. A. (2008). *Aerosol optics: Light absorption and scattering by particles in the atmosphere*. Springer Science & Business Media.

Könemann, T., Savage, N., Klimach, T., Walter, D., Fröhlich-Nowoisky, J., Su, H., et al. (2019). Spectral intensity bioaerosol sensor (SIBS): An instrument for spectrally resolved fluorescence detection of single particles in real time. *Atmospheric Measurement Techniques*, *12*(2), 1337–1363. https://doi.org/10.5194/amt-12-1337-2019

Kucera, M. (2007). Chapter six planktonic foraminifera as tracers of past oceanic environments. In C. Hillaire-Marcel & A. De Vernal (Eds.), *Proxies in late Cenozoic paleoceanography* (Vol. 1, pp. 213–262). Elsevier. https://doi.org/10.1016/S1572-5480(07)01011-1

Kunert, A. T., Lamneck, M., Helleis, F., Pöschl, U., Pöhlker, M. L., & Fröhlich-Nowoisky, J. (2018). Twin-plate Ice Nucleation Assay (TINA) with infrared detection for high-throughput droplet freezing experiments with biological ice nuclei in laboratory and field samples. *Atmospheric Measurement Techniques*, *11*(11), 6327–6337. https://doi.org/10.5194/amt-11-6327-2018

Lang-Yona, N., Flores, J. M., Haviv, R., Alberti, A., Poulain, J., Belser, C., et al. (2022). Terrestrial and marine influence on atmospheric bacterial diversity over the north Atlantic and Pacific Oceans. *Communications Earth & Environment*, *3*(1), 121. https://doi.org/10.1038/s43247-022-00441-6

Laurent, B., Marticorena, B., Bergametti, G., Léon, J. F., & Mahowald, N. M. (2008). Modeling mineral dust emissions from the Sahara Desert using new surface properties and soil database. *Journal of Geophysical Research*, *113*(D14), D14218. https://doi.org/10.1029/2007JD009484

Lefèvre, N., Veleda, D., & Hartman, S. E. (2023). Outgassing of CO_2 dominates in the coastal upwelling off the northwest African coast. *Deep Sea Research Part I: Oceanographic Research Papers*, *200*, 104130. https://doi.org/10.1016/j.dsr.2023.104130

Leibold, P., & Al Abri, O. (2019). An integrated web-based approach for near real-time mission monitoring. In *2019 1st international conference on unmanned vehicle systems-Oman (UVS)* (pp. 1–6). IEEE. https://doi.org/10.1109/UVS.2019.8658284

Leibold, P., Diller, N., Reißmann, S., & Faber, C. (2023). Beluga: An integrated marine multi-platform infrastructure and near real-time Ocean Data visualization tool. In *Oceans 2023—MTS/IEEE U.S. Gulf coast, Biloxi, MS, USA, 2023* (pp. 1–10). https://doi.org/10.23919/OCEANS52994.2023.10337372

Longhurst, A. R. (2007). *Ecological geography of the sea* (2nd ed.). Academic Press.

Löscher, C. R., Bange, H. W., Schmitz, R. A., Callbeck, C. M., Engel, A., Hauss, H., et al. (2016). Water column biogeochemistry of oxygen minimum zones in the eastern tropical North Atlantic and eastern tropical South Pacific oceans. *Biogeosciences*, *13*(12), 3585–3606. https://doi.org/10.5194/bg-13-3585-2016

Marrec, P., Grégori, G., Doglioli, A. M., Dugenne, M., Della Penna, A., Bhairy, N., et al. (2018). Coupling physics and biogeochemistry thanks to high-resolution observations of the phytoplankton community structure in the northwestern Mediterranean Sea. *Biogeosciences*, *15*(5), 1579–1606. https://doi.org/10.5194/bg-15-1579-2018

Martin, J. H., & Fitzwater, S. E. (1988). Iron deficiency limits phytoplankton growth in the north-east Pacific subarctic. *Nature*, *331*(6154), 341–343. https://doi.org/10.1038/331341a0

Martínez-García, A., Rosell-Melé, A., Geibert, W., Gersonde, R., Masqué, P., Gaspari, V., & Barbante, C. (2009). Links between iron supply, marine productivity, sea surface temperature, and CO_2 over the last 1.1 Ma. *Paleoceanography*, *24*(1). https://doi.org/10.1029/2008PA001657

Martínez-García, A., Sigman, D. M., Ren, H., Anderson, R. F., Straub, M., Hodell, D. A., et al. (2014). Iron fertilization of the subantarctic ocean during the last ice age. *Science*, *343*(6177), 1347–1350. https://doi.org/10.1126/science.1246848

Mayol, E., Arrieta, J. M., Jiménez, M. A., Martínez-Asensio, A., Garcias-Bonet, N., Dachs, J., et al. (2017). Long-range transport of airborne microbes over the global tropical and subtropical ocean. *Nature Communications*, *8*(1), 201. https://doi.org/10.1038/s41467-017-00110-9

McCoy, D. T., Burrows, S. M., Wood, R., Grosvenor, D. P., Elliott, S. M., Ma, P.-L., et al. (2015). Natural aerosols explain seasonal and spatial patterns of Southern Ocean cloud albedo. *Science Advances*, *1*(6), e1500157. https://doi.org/10.1126/sciadv.1500157

Meskhidze, N., Petters, M. D., Tsigaridis, K., Bates, T., O'Dowd, C., Reid, J., et al. (2013). Production mechanisms, number concentration, size distribution, chemical composition, and optical properties of sea spray aerosols: Production and properties of sea spray aerosol. *Atmospheric Science Letters*, *14*(4), 207–213. https://doi.org/10.1002/asl2.441

Mohtadi, M., Steinke, S., Groeneveld, J., Fink, H. G., Rixen, T., Hebbeln, D., et al. (2009). Low-latitude control on seasonal and interannual changes in planktonic foraminiferal flux and shell geochemistry off south Java. *Paleoceanography*, *24*(1). https://doi.org/10.1029/2008PA001636

Monks, P. S., Granier, C., Fuzzi, S., Stohl, A., Williams, M. L., Akimoto, H., et al. (2009). Atmospheric composition change—Global and regional air quality. *Atmospheric Environment*, *43*(33), 5268–5350. https://doi.org/10.1016/j.atmosenv.2009.08.021

Moon, W., Kim, B.-M., Yang, G.-H., & Wettlaufer, J. S. (2022). Wavier jet streams driven by zonally asymmetric surface thermal forcing. *Proceedings of the National Academy of Sciences*, *119*(38), e2200890119. https://doi.org/10.1073/pnas.2200890119

Moore, J. K., Fu, W., Primeau, F., Britten, G. L., Lindsay, K., Long, M., et al. (2018). Sustained climate warming drives declining marine biological productivity. *Science*, *359*(6380), 1139–1143. https://doi.org/10.1126/science.aao6379

Moore, M., Mills, M. M., Achterberg, E. P., Geider, R. J., LaRoche, J., Lucas, M. I., et al. (2009). Large-scale distribution of Atlantic nitrogen fixation controlled by iron availability. *Nature Geoscience*, *2*(12), 867–871. https://doi.org/10.1038/ngeo667

Morris, C. E., Conen, F., Alex Huffman, J., Phillips, V., Pöschl, U., & Sands, D. C. (2014). Bioprecipitation: A feedback cycle linking Earth history, ecosystem dynamics and land use through biological ice nucleators in the atmosphere. *Global Change Biology*, *20*(2), 341–351. https://doi.org/10.1111/gcb.12447

Mulitza, S., Bickert, T., Bostock, H. C., Chiessi, C. M., Donner, B., Govin, A., et al. (2022). World Atlas of late quaternary foraminiferal oxygen and carbon isotope ratios. *Earth System Science Data*, *14*(6), 2553–2611. https://doi.org/10.5194/essd-14-2553-2022

Müller, P. J., Čepek, M., Ruhland, G., & Schneider, R. R. (1997). Alkenone and coccolithophorid species changes in late Quaternary sediments from the Walvis Ridge: Implications for the alkenone paleotemperature method. *Palaeogeography, Palaeoclimatology, Palaeoecology*, *135*(1–4), 71–96. https://doi.org/10.1016/S0031-0182(97)00018-7

Nencioli, F., Dong, C., Dickey, T., Washburn, L., & McWilliams, J. C. (2010). A vector geometry–based eddy detection algorithm and its application to a high-resolution numerical model product and high-frequency radar surface velocities in the southern California bight. *Journal of Atmospheric and Oceanic Technology*, *27*(3), 564–579. https://doi.org/10.1175/2009JTECHO725.1

Nürnberg, D., Bijma, J., & Hemleben, C. (1996). Assessing the reliability of magnesium in foraminiferal calcite as a proxy for water mass temperatures. *Geochimica et Cosmochimica Acta*, *60*(5), 803–814. https://doi.org/10.1016/0016-7037(95)00446-7

O'Dowd, C. D., & de Leeuw, G. (2007). Marine aerosol production: A review of the current knowledge. *Philosophical Transactions of the Royal Society A: Mathematical, Physical & Engineering Sciences*, *365*(1856), 1753–1774. https://doi.org/10.1098/rsta.2007.2043

Pabortsava, K., Lampitt, R. S., Benson, J., Crowe, C., McLachlan, R., Le Moigne, F. A. C., et al. (2017). Carbon sequestration in the deep Atlantic enhanced by Saharan dust. *Nature Geoscience*, *10*(3), 189–194. https://doi.org/10.1038/ngeo2899

Partensky, F., Blanchot, J., & Vaulot, D. (1999). Differential distribution and ecology of Prochlorococcus and Synechococcus in oceanic waters: A review.

Pesant, S., Not, F., Picheral, M., Kandels-Lewis, S., Le Bescot, N., Gorsky, G., et al. (2015). Open science resources for the discovery and analysis of Tara Oceans data. *Scientific Data*, *2*(1), 150023. https://doi.org/10.1038/sdata.2015.23

Petäjä, T., Mordas, G., Manninen, H., Aalto, P. P., Hämeri, K., & Kulmala, M. (2006). Detection efficiency of a water-based TSI condensation particle counter 3785. *Aerosol Science and Technology*, *40*(12), 1090–1097. https://doi.org/10.1080/02786820600979139

Pöschl, U. (2005). Atmospheric aerosols: Composition, transformation, climate and health effects. *Angewandte Chemie International Edition*, *44*(46), 7520–7540. https://doi.org/10.1002/anie.200501122

Poulton, A. J., Holligan, P. M., Hickman, A., Kim, Y.-N., Adey, T. R., Stinchcombe, M. C., et al. (2006). Phytoplankton carbon fixation, chlorophyll-biomass and diagnostic pigments in the Atlantic Ocean. *Deep Sea Research Part II: Topical Studies in Oceanography*, *53*(14–16), 1593–1610. https://doi.org/10.1016/j.dsr2.2006.05.007

Prahl, F. G., & Wakeham, S. G. (1987). Calibration of unsaturation patterns in long-chain ketone compositions for palaeotemperature assessment. *Nature*, *330*(6146), 367–369. https://doi.org/10.1038/330367a0

Prass, M., Andreae, M. O., de Araùjo, A. C., Artaxo, P., Ditas, F., Elbert, W., et al. (2021). Bioaerosols in the Amazon rain forest: Temporal variations and vertical profiles of Eukarya, bacteria, and Archaea. *Biogeosciences*, *18*(17), 4873–4887. https://doi.org/10.5194/bg-18-4873-2021

Prather, K. A., Bertram, T. H., Grassian, V. H., Deane, G. B., Stokes, M. D., DeMott, P. J., et al. (2013). Bringing the ocean into the laboratory to probe the chemical complexity of sea spray aerosol. *Proceedings of the National Academy of Sciences*, *110*(19), 7550–7555. https://doi.org/10.1073/pnas.1300262110

Prospero, J. M., Barkley, A. E., Gaston, C. J., Gatineau, A., Campos y Sansano, A., & Panechou, K. (2020). Characterizing and quantifying African dust transport and deposition to South America: Implications for the phosphorus budget in the Amazon Basin. *Global Biogeochemical Cycles*, *34*(9), e2020GB006536. https://doi.org/10.1029/2020GB006536

Raghavan, V., Eichele, G., Larink, O., Karin, E. L., & Söding, J. (2023). RNA sequencing indicates widespread conservation of circadian clocks in marine zooplankton. https://doi.org/10.1093/nar/gkn000

Ramachandran, S. (2018). Aerosols and climate change: Present understanding, challenges, and future outlook. In K. P. Vadrevu, T. Ohara, & C. Justice (Eds.), *Land-atmospheric research applications in South and Southeast Asia* (pp. 341–378). Springer International Publishing. https://doi.org/10.1007/978-3-319-67474-2_17

Ramanathan, V., Crutzen, P. J., Kiehl, J. T., & Rosenfeld, D. (2001). Aerosols, climate, and the hydrological cycle. *Science*, *294*(5549), 2119–2124. https://doi.org/10.1126/science.1064034

Ren, H., Sigman, D. M., Meckler, A. N., Plessen, B., Robinson, R. S., Rosenthal, Y., & Haug, G. H. (2009). Foraminiferal isotope evidence of reduced nitrogen fixation in the ice Age Atlantic Ocean. *Science*, *323*(5911), 244–248. https://doi.org/10.1126/science.1165787

Resplandy, L. (2018). Will ocean zones with low oxygen levels expand or shrink? *Nature*, *557*(7705), 314–315. https://doi.org/10.1038/d41586-018-05034-y

Reygondeau, G., & Dunn, D. (2019). Pelagic biogeography. In *Encyclopedia of ocean sciences* (pp. 588–598). Elsevier. https://doi.org/10.1016/B978-0-12-409548-9.11633-1

Richey, J. N., & Tierney, J. E. (2016). GDGT and alkenone flux in the northern Gulf of Mexico: Implications for the TEX_{86} and $U^{K'}_{37}$ paleothermometers: GDGT and alkenone flux in Gulf of Mexico. *Paleoceanography*, *31*(12), 1547–1561. https://doi.org/10.1002/2016PA003032

Rinaldi, M., Decesari, S., Carbone, C., Finessi, E., Fuzzi, S., Ceburnis, D., et al. (2011). Evidence of a natural marine source of oxalic acid and a possible link to glyoxal. *Journal of Geophysical Research*, *116*(D16), D16204. https://doi.org/10.1029/2011JD015659

Robinson, R. S., Kienast, M., Luiza Albuquerque, A., Altabet, M., Contreras, S., De Pol Holz, R., et al. (2012). A review of nitrogen isotopic alteration in marine sediments. *Paleoceanography*, *27*(4), 1–13. https://doi.org/10.1029/2012PA002321

Rodriguez-Caballero, E., Belnap, J., Büdel, B., Crutzen, P. J., Andreae, M. O., Pöschl, U., & Weber, B. (2018). Dryland photoautotrophic soil surface communities endangered by global change. *Nature Geoscience*, *11*(3), 185–189. https://doi.org/10.1038/s41561-018-0072-1

Rodriguez-Caballero, E., Stanelle, T., Egerer, S., Cheng, Y., Su, H., Canton, Y., et al. (2022). Global cycling and climate effects of aeolian dust controlled by biological soil crusts. *Nature Geoscience*, *15*(6), 458–463. https://doi.org/10.1038/s41561-022-00942-1

Rosell-Melé, A., & Prahl, F. G. (2013). Seasonality of U K ′ 37 temperature estimates as inferred from sediment trap data. *Quaternary Science Reviews*, *72*, 128–136. https://doi.org/10.1016/j.quascirev.2013.04.017

Sadekov, A., Eggins, S. M., De Deckker, P., Ninnemann, U., Kuhnt, W., & Bassinot, F. (2009). Surface and subsurface seawater temperature reconstruction using Mg/Ca microanalysis of planktonic foraminifera *Globigerinoides ruber*, *Globigerinoides sacculifer*, and *Pulleniatina obliquiloculata*: Seawater temperature reconstruction. *Paleoceanography*, *24*(3), PA3201. https://doi.org/10.1029/2008PA001664

Schiebel, R. (2002). Planktic foraminiferal sedimentation and the marine calcite budget. *Global Biogeochemical Cycles*, *16*(4), 3-1–3-21. https://doi.org/10.1029/2001GB001459

Schiebel, R. (2024). Data from probing the open ocean with the research sail yacht *Eugen Seibold* [Dataset]. *Edmond*. https://doi.org/10.17617/3.30MFES

Schiebel, R., & Hemleben, C. (2000). Interannual variability of planktic foraminiferal populations and test flux in the eastern North Atlantic Ocean (JGOFS). *Deep Sea Research Part II: Topical Studies in Oceanography*, *47*(9–11), 1809–1852. https://doi.org/10.1016/S0967-0645(00)00008-4

Schiebel, R., & Hemleben, C. (2017). *Planktic foraminifers in the modern ocean: Ecology, biogeochemistry, and application*. Springer. https://doi.org/10.1007/978-3-662-50297.6

Schiebel, R., & Movellan, A. (2012). First-order estimate of the planktic foraminifer biomass in the modern ocean. *Earth System Science Data*, *4*(1), 75–89. https://doi.org/10.5194/essd-4-75-2012

Schiebel, R., Smart, S. M., Jentzen, A., Jonkers, L., Morard, R., Meilland, J., et al. (2018). Advances in planktonic foraminifer research: New perspectives for paleoceanography. *Revue de Micropaleontologie*, *61*(3–4), 113–138. https://doi.org/10.1016/j.revmic.2018.10.001

Schlitzer, R. (2022). Ocean data view (version 5.6.3). Retrieved from odv.awi.de

Schmidtko, S., Stramma, L., & Visbeck, M. (2017). Decline in global oceanic oxygen content during the past five decades. *Nature*, *542*(7641), 335–339. https://doi.org/10.1038/nature21399

Schouten, S., Hopmans, E. C., Schefuß, E., & Sinninghe Damsté, J. S. (2002). Distributional variations in marine crenarchaeotal membrane lipids: A new tool for reconstructing ancient sea water temperatures? *Earth and Planetary Science Letters*, *204*(1–2), 265–274. https://doi.org/10.1016/S0012-821X(02)00979-2

Schouten, S., Hopmans, E. C., & Sinninghe Damsté, J. S. (2013). The organic geochemistry of glycerol dialkyl glycerol tetraether lipids: A review. *Organic Geochemistry*, *54*, 19–61. https://doi.org/10.1016/j.orggeochem.2012.09.006

Schwab, V. F., Garcin, Y., Sachse, D., Todou, G., Séné, O., Onana, J.-M., et al. (2015). Effect of aridity on $\delta^{13}C$ and δD values of C3 plant- and C4 graminoid-derived leaf wax lipids from soils along an environmental gradient in Cameroon (Western Central Africa). *Organic Geochemistry*, *78*, 99–109. https://doi.org/10.1016/j.orggeochem.2014.09.007

Schwarz, J. P., Gao, R. S., Fahey, D. W., Thomson, D. S., Watts, L. A., Wilson, J. C., et al. (2006). Single-particle measurements of midlatitude black carbon and light-scattering aerosols from the boundary layer to the lower stratosphere. *Journal of Geophysical Research*, *111*(D16), D16207. https://doi.org/10.1029/2006JD007076

Shi, H., Jin, F.-F., Wills, R. C. J., Jacox, M. G., Amaya, D. J., Black, B. A., et al. (2022). Global decline in ocean memory over the 21st century. *Science Advances*, *8*(18), eabm3468. https://doi.org/10.1126/sciadv.abm3468

Siccha, M., & Kucera, M. (2017). ForCenS, a curated database of planktonic foraminifera census counts in marine surface sediment samples. *Scientific Data*, *4*(1), 170109. https://doi.org/10.1038/sdata.2017.109

Siegel, D., & Deuser, W. (1997). Trajectories of sinking particles in the Sargasso sea: Modeling of statistical funnels above deep-ocean sediment traps. *Deep Sea Research Part I: Oceanographic Research Papers*, *44*(9–10), 1519–1541. https://doi.org/10.1016/s0967-0637(97)00028-9

Sigman, D. M., & Haug, G. H. (2003). The biological pump in the past. In *Treatise on Geochemistry* (pp. 491–528). Elsevier. https://doi.org/10.1016/B0-08-043751-6/06118-1

Sigman, D. M., Karsh, K. L., & Casciotti, K. L. (2009). Nitrogen isotopes in the Ocean. In *Encyclopedia of ocean Sciences* (pp. 40–54). Elsevier. https://doi.org/10.1016/B978-012374473-9.00632-9

Sigman, O. M., Altabet, M. A., McCorkle, D. C., Francois, R., & Fischer, G. (1999). The $\delta^{15}N$ of nitrate in the Southern Ocean: Consumption of nitrate in surface waters. *Global Biogeochemical Cycles*, *13*(4), 1149–1166. https://doi.org/10.1029/1999GB900038

Smart, S. M., Fawcett, S. E., Ren, H., Schiebel, R., Tompkins, E. M., Martínez-García, A., et al. (2020). The nitrogen isotopic composition of tissue and shell-bound organic matter of planktic foraminifera in Southern Ocean surface waters. *Geochemistry, Geophysics, Geosystems*, *21*(2), 1–29. https://doi.org/10.1029/2019GC008440

Smart, S. M., Ren, H., Fawcett, S. E., Schiebel, R., Conte, M., Rafter, P. A., et al. (2018). Ground-truthing the planktic foraminifer-bound nitrogen isotope paleo-proxy in the Sargasso Sea. *Geochimica et Cosmochimica Acta*, *235*, 463–482. https://doi.org/10.1016/j.gca.2018.05.023

Souza, F. F. C., Mathai, P. P., Pauliquevis, T., Balsanelli, E., Pedrosa, F. O., Souza, E. M., et al. (2021). Influence of seasonality on the aerosol microbiome of the Amazon rainforest. *Science of the Total Environment*, *760*, 144092. https://doi.org/10.1016/j.scitotenv.2020.144092

Spero, H. J., & Williams, D. F. (1988). Extracting environmental information from planktonic foraminiferal $\delta^{13}C$ data. *Nature*, *335*(6192), 717–719. https://doi.org/10.1038/335717a0

Steffen, W., Richardson, K., Rockström, J., Schellnhuber, H. J., Dube, O. P., Dutreuil, S., et al. (2020). The emergence and evolution of Earth System Science. *Nature Reviews Earth & Environment*, *1*(1), 54–63. https://doi.org/10.1038/s43017-019-0005-6

Stramma, L., Johnson, G. C., Sprintall, J., & Mohrholz, V. (2008). Expanding oxygen-minimum zones in the tropical oceans. *Science*, *320*(5876), 655–658. https://doi.org/10.1126/science.1153847

Su, H., Cheng, Y., & Pöschl, U. (2020). New Multiphase chemical processes influencing atmospheric aerosols, air quality, and climate in the anthropocene. *Accounts of Chemical Research*, *53*(10), 2034–2043. https://doi.org/10.1021/acs.accounts.0c00246

Suggett, D., Moore, C., Hickman, A., & Geider, R. (2009). Interpretation of fast repetition rate (FRR) fluorescence: Signatures of phytoplankton community structure versus physiological state. *Marine Ecology Progress Series*, *376*, 1–19. https://doi.org/10.3354/meps07830

Sunda, W. G. (2012). Feedback interactions between trace metal nutrients and phytoplankton in the Ocean. *Frontiers in Microbiology*, *3*, 204. https://doi.org/10.3389/fmicb.2012.00204

Sutton, T. T., Clark, M. R., Dunn, D. C., Halpin, P. N., Rogers, A. D., Guinotte, J., et al. (2017). A global biogeographic classification of the mesopelagic zone. *Deep Sea Research Part I: Oceanographic Research Papers*, *126*, 85–102. https://doi.org/10.1016/j.dsr.2017.05.006

Taylor, K. W. R., Huber, M., Hollis, C. J., Hernandez-Sanchez, M. T., & Pancost, R. D. (2013). Re-evaluating modern and Palaeogene GDGT distributions: Implications for SST reconstructions. *Global and Planetary Change*, *108*, 158–174. https://doi.org/10.1016/j.gloplacha.2013.06.011

Thomson, W., & Murray, J. (1886). Report on the scientific results of the Voyage of HMS "Challenger" during the Years 1873–76 under the Command of Capt G. S. Nares, R.N., F.R.S., and Capt F. T. Thomson, R.N. *Nature*, *35*(890), 49–51. https://doi.org/10.1038/035049a0

Thunell, R. C., Sigman, D. M., Muller-Karger, F., Astor, Y., & Varela, R. (2004). Nitrogen isotope dynamics of the Cariaco basin, Venezuela: Cariaco basin nitrogen isotopes. *Global Biogeochemical Cycles*, *18*(3), GB3001. https://doi.org/10.1029/2003GB002185

Timmermann, A., Yun, K.-S., Raia, P., Ruan, J., Mondanaro, A., Zeller, E., et al. (2022). Climate effects on archaic human habitats and species successions. *Nature*, *604*(7906), 495–501. https://doi.org/10.1038/s41586-022-04600-9

Twining, B. S., & Baines, S. B. (2013). The trace metal composition of marine phytoplankton. *Annual Review of Marine Science*, *5*(1), 191–215. https://doi.org/10.1146/annurev-marine-121211-172322

van de Poll, W. H., Kulk, G., Timmermans, K. R., Brussaard, C. P. D., van der Woerd, H. J., Kehoe, M. J., et al. (2013). Phytoplankton chlorophyll *a* biomass, composition, and productivity along a temperature and stratification gradient in the northeast Atlantic Ocean. *Biogeosciences*, *10*(6), 4227–4240. https://doi.org/10.5194/bg-10-4227-2013

Vaulot, D., Eikrem, W., Viprey, M., & Moreau, H. (2008). The diversity of small eukaryotic phytoplankton (≤3 μm) in marine ecosystems. *FEMS Microbiology Reviews*, *32*(5), 795–820. https://doi.org/10.1111/j.1574-6976.2008.00121.x

Vincent, E., & Berger, W. (1981). Planktonic foraminifera and their use in paleoceanography. *The Sea*, *7*, 1025–1119.

Völker, A. H. L., Sarnthein, M., Grootes, P. M., Erlenkeuser, H., Laj, C., Mazaud, A., et al. (1998). Correlation of marine ^{14}C Ages from the Nordic seas with the GISP2 isotope record: Implications for 14C calibration beyond 25 ka BP. *Radiocarbon*, *40*(1), 517–534. https://doi.org/10.1017/S0033822200018397

von der Weiden, S.-L., Drewnick, F., & Borrmann, S. (2009). Particle loss calculator—A new software tool for the assessment of the performance of aerosol inlet systems. *Atmospheric Measurement Techniques*, *2*(2), 479–494. https://doi.org/10.5194/amt-2-479-2009

Vonhof, H. B., de Graaf, S., Spero, H. J., Schiebel, R., Verdegaal, S. J. A., Metcalfe, B., & Haug, G. H. (2020). High-precision stable isotope analysis of <5 μg $CaCO_3$ samples by continuous-flow mass spectrometry. *Rapid Communications in Mass Spectrometry*, *34*(19), e8878. https://doi.org/10.1002/rcm.8878

von Schuckmann, K., Cheng, L., Palmer, M. D., Hansen, J., Tassone, C., Aich, V., et al. (2020). Heat stored in the Earth system: Where does the energy go? *Earth System Science Data*, *12*(3), 2013–2041. https://doi.org/10.5194/essd-12-2013-2020

Walter, D., Aardema, H. M., Calleja, M. L., Dragoneas, A., Hrabe de Angelis, I., Pöhlker, C., et al. (2023). Master track of *Eugen Seibold* cruise ES19C01, Playa Blanca—Caniçal, 2019-04-08—2019-04-10 [Dataset]. *Max Planck Institute for Chemistry, PANGAEA*. https://doi.org/10.1594/PANGAEA.960382

Wilkinson, M. D., Dumontier, M., Aalbersberg, I. J., Appleton, G., Axton, M., Baak, A., et al. (2016). The FAIR Guiding Principles for scientific data management and stewardship. *Scientific Data*, *3*(1), 160018. https://doi.org/10.1038/sdata.2016.18

Williamson, C. J., Kupc, A., Axisa, D., Bilsback, K. R., Bui, T., Campuzano-Jost, P., et al. (2019). A large source of cloud condensation nuclei from new particle formation in the tropics. *Nature*, *574*(7778), 399–403. https://doi.org/10.1038/s41586-019-1638-9

Wuchter, C., Schouten, S., Wakeham, S. G., & Sinninghe Damsté, J. S. (2005). Temporal and spatial variation in tetraether membrane lipids of marine Crenarchaeota in particulate organic matter: Implications for TEX_{86} paleothermometry: Temporal and spatial variation in TEX_{86}. *Paleoceanography*, *20*(3), PA3013. https://doi.org/10.1029/2004PA001110

Yu, Y., Kalashnikova, O. V., Garay, M. J., Lee, H., Notaro, M., Campbell, J. R., et al. (2020). Disproving the Bodélé depression as the primary source of dust fertilizing the Amazon Rainforest. *Geophysical Research Letters*, *47*(13), e2020GL088020. https://doi.org/10.1029/2020GL088020

Zanna, L., Khatiwala, S., Gregory, J. M., Ison, J., & Heimbach, P. (2019). Global reconstruction of historical ocean heat storage and transport. *Proceedings of the National Academy of Sciences*, *116*(4), 1126–1131. https://doi.org/10.1073/pnas.1808838115

Zheng, G., Wang, Y., Wood, R., Jensen, M. P., Kuang, C., McCoy, I. L., et al. (2021). New particle formation in the remote marine boundary layer. *Nature Communications*, *12*(1), 527. https://doi.org/10.1038/s41467-020-20773-1

Zonneveld, K. A. F., Versteegh, G. J. M., Kasten, S., Eglinton, T. I., Emeis, K.-C., Huguet, C., et al. (2010). Selective preservation of organic matter in marine environments; processes and impact on the sedimentary record. *Biogeosciences*, *7*(2), 483–511. https://doi.org/10.5194/bg-7-483-2010